

RESEARCH ARTICLE

10.1002/2016JC012665

Special Section:

Dense Water Formations in the North Western Mediterranean: From the Physical Forcings to the Biogeochemical Consequences

Key Points:

- Modeling of annual nitrogen and phosphorus cycles in the northwestern Mediterranean deep convection region for the period 2012–2013
- The deep convection area was a sink of inorganic matter and a source of organic matter for the surrounding area over the period 2012–2013
- The N:P ratio in the surface layer is submitted to drastic variations during deep convection and bloom transition periods

Supporting Information:

- Supporting Information S1
- Table S1

Correspondence to:

F. Kessouri,
kesf@ucla.edu

Citation:

Kessouri, F., Ulses, C., Estournel, C., Marsaleix, P., Severin, T., Pujo-Pay, M., . . . Conan, P. (2017). Nitrogen and phosphorus budgets in the northwestern Mediterranean deep convection region. *Journal of Geophysical Research: Oceans*, 122, 9429–9454. <https://doi.org/10.1002/2016JC012665>

Received 27 DEC 2016












Accepted 21 AUG 2017

Accepted article online 2 NOV 2017

Published online 5 DEC 2017

© 2017. American Geophysical Union.
All Rights Reserved.

Nitrogen and Phosphorus Budgets in the Northwestern Mediterranean Deep Convection Region

Faycal Kessouri^{1,2,3} , Caroline Ulses¹ , Claude Estournel¹ , Patrick Marsaleix¹ , Tatiana Severin⁴ , Mireille Pujo-Pay⁵, Jocelyne Caparros⁵, Patrick Raimbault⁶ , Orens Pasqueron de Fommervault⁷ , Fabrizio D'Ortenzio⁷ , Vincent Taillandier⁷ , Pierre Testor⁸ , and Pascal Conan⁵ 

¹Laboratoire d'Aérodologie, Université de Toulouse, CNRS, UPS, Laboratoire d'Aérodologie, Toulouse, France, ²Department of Atmospheric and Oceanic Sciences, University of California Los Angeles, Los Angeles, CA, USA, ³Department of Biogeochemistry, Southern California Coastal Water Research Project, Costa Mesa, CA, USA, ⁴Marine Science Institute, University of Texas at Austin, Port Aransas, TX, USA, ⁵Laboratoire d'Océanographie Microbienne, Banyuls sur Mer, France, ⁶Institut Méditerranéen d'Océanologie, Marseille, France, ⁷Sorbonne Universités, UPMC Univ. Paris 06, and CNRS UMR 7093, LOV, Observatoire océanologique, Villefranche sur Mer, France, ⁸CNRS/LOCEAN, Paris, France

Abstract The aim of this study is to understand the biogeochemical cycles of the northwestern Mediterranean Sea (NW Med), where a recurrent spring bloom related to dense water formation occurs. We used a coupled physical-biogeochemical model at high resolution to simulate realistic 1 year period and analyze the nitrogen (N) and phosphorus (P) cycles. First, the model was evaluated using cruises carried out in winter, spring, and summer and a Bio-Argo float deployed in spring. Then, the annual cycle of meteorological and hydrodynamical forcing and nutrients stocks in the upper layer were analyzed. Third, the effect of biogeochemical and physical processes on N and P was quantified. Fourth, we quantified the effects of the physical and biological processes on the seasonal changes of the molar NO₃:PO₄ ratio, particularly high compared to the global ocean. The deep convection reduced the NO₃:PO₄ ratio of upper waters, but consumption by phytoplankton increased it. Finally, N and P budgets were estimated. At the annual scale, this area constituted a sink of inorganic and a source of organic N and P for the peripheral area. NO₃ and PO₄ were horizontally advected from the peripheral regions into the intermediate waters (130–800 m) of the deep convection area, while organic matter was exported throughout the whole water column toward the surrounding areas. The annual budget suggests that the NW Med deep convection constitutes a major source of nutrients for the photic zone of the Mediterranean Sea.

1. Introduction

The Mediterranean Sea, often considered as an oligotrophic region (Antoine et al., 2005), exhibits nutrient-depleted surface waters most of the year and low nutrient concentrations in deep waters (Krom et al., 1991). With respect to the global ocean Redfield nitrate (NO₃) to phosphate (PO₄) ratio of 16:1 (Redfield, 1964), the Mediterranean Sea is characterized by particularly high values (Ribera d'Alcalà et al., 2003). Moreover, these oligotrophic conditions and high NO₃:PO₄ (hereafter N:P) ratios show a pronounced east-west gradient (Pujo-Pay et al., 2011), with the eastern basin presenting ultra-oligotrophic conditions. The N:P ratios in deep layers were estimated at 20–22 in the western subbasin (Béthoux et al., 1998) and at 27–30 in the eastern subbasin (Ribera d'Alcalà et al., 2003) of the Mediterranean.

The distribution of nutrients in the semienclosed Mediterranean Sea results from internal physical and biogeochemical dynamics, from atmospheric and terrestrial inputs, and from exchanges with the Atlantic Ocean and the Black Sea. Physical dynamics are partly controlled by the formation of intermediate and deep waters as the winter climate of the Mediterranean Sea is characterized by cold, dry local winds blowing from the north (Hauser et al., 2003), which induce an increase of the surface layer density by strong evaporation and cooling, and then trigger the deep convection mixing. This process is responsible for the formation of intermediate and deep water masses in the northwestern basin (hereafter NW Med; Medoc Group, 1970), the south Adriatic (Pollak, 1951), the Aegean (Nittis et al., 2003), and the Rhodes Gyre (Ovchinnikov, 1984). The high nitrate and phosphate surface concentrations (values close to deep concentrations)

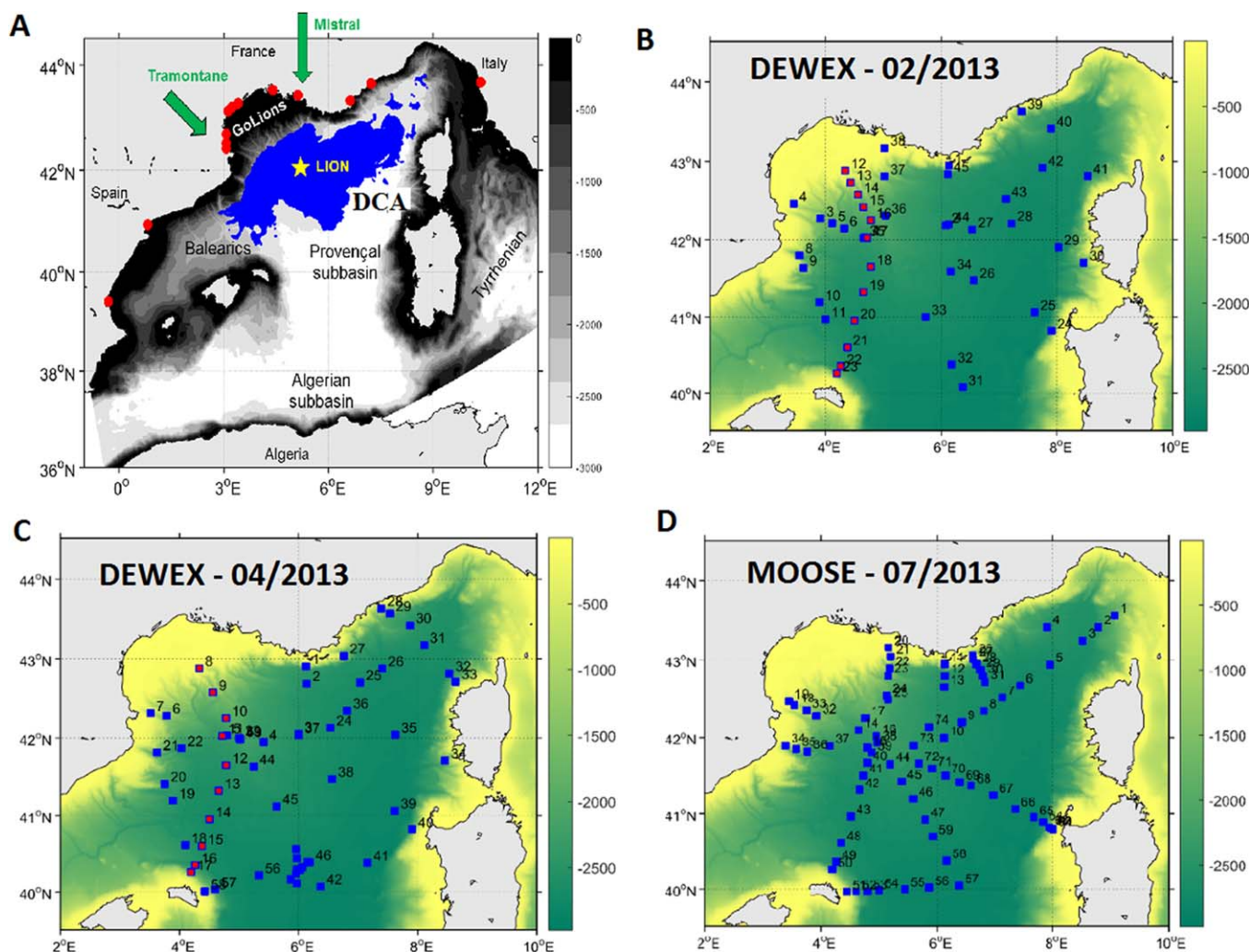


Figure 1. (a) Bathymetry (m) of the coupled physical-biogeochemical model domain. The red dots represent the modeled river locations. The blue area DCA (deep convection area) corresponds to the simulation analysis area. The yellow star corresponds to the LION station where the heat flux plotted in Figure 6 was modeled. The biogeochemical measurement stations of the (b) DeWEX Leg 1 (February 2013), (c) DeWEX Leg 2 (April 2013), and (d) MOOSE-GE 2013 (July 2013) cruises. Stations in red in Figures 1b and 1c are located in the transect presented in Figures 3 and 4.

observed during convective episodes in these regions (Gačić et al., 2002; Santinelli et al., 2012; Severin et al., 2014; Yilmaz & Tugrul, 1998) demonstrate that the deep convection process is also responsible for large nutrient enrichments of the upper layers. In addition, a study based on satellite-derived chlorophyll *a* data (D’Ortenzio & Ribera d’Alcalà, 2009) has shown that the deep convection regions are characterized by intense to moderate spring blooms, while phytoplankton development in the rest of the open Mediterranean Sea is of low magnitude. This feature of phytoplankton dynamics in convection regions may be explained by the large amounts of nutrient supplied during the intense vertical mixing events (Lavigne et al., 2015).

Among the deep convection regions of the Mediterranean Sea, the NW Med (Figure 1a) has been identified as the region where the vertical mixing and the associated phytoplankton spring bloom are the most intense and recurrent (D’Ortenzio & Ribera d’Alcalà, 2009; Houpert et al., 2015; Lavigne, 2013; Mayot et al., 2016). The NW Med convection has been shown to largely influence the regional biogeochemical cycles and marine ecosystems, mostly by importing nutrient-enriched deep waters to the surface (Severin et al., 2014; Ulses et al., 2016). This enrichment changes the biogeochemical characteristics of the surface layers (Auger et al., 2014; Durrieu de Madron & Mermex Group, 2011; Herrmann et al., 2013), induces a large phytoplankton spring bloom (D’Ortenzio & Ribera d’Alcalà, 2009; Estrada et al., 2014; Lavigne, 2013), favors high

particulate carbon export (Gogou et al., 2014; Ulses et al., 2016), and shifts the zooplankton community toward larger sized organisms (Auger et al., 2014). Moreover, deep convection in the NW Med has also been shown to promote a change of the surface nutrient ratios (Pasqueron de Fommervault et al., 2015a; Severin et al., 2014). However, the impact of nutrient replenishments on the seasonal cycles of nitrogen and phosphorus has been poorly explored. The few quantifications of the upward flux of nitrate and phosphate that have been performed (Severin et al., 2014; Ulses et al., 2016) remain limited in space and/or time. A thorough quantification of the processes linked to the seasonal variations of nitrogen and phosphorus cycles during one complete year has not yet been proposed in this region.

The objectives of the DeWEX project (Deep Water formation EXperiment) are (i) to better understand the impact of dense water formation on the marine biogeochemical cycles and (ii) to provide a consistent data set of hydrological and biogeochemical parameters to improve the numerical modeling of the convection hydrology and coupled biogeochemical processes. To fulfill these objectives, oceanographic research vessels covered the deep convection area during each season from summer 2012 to summer 2013. Once calibrated and validated, numerical modeling is expected to achieve goals at different time scales. In the short term, the model is expected to interpolate between the DeWEX cruises to calculate the nutrient and organic matter budgets over an annual cycle. In the long term, and after complementary validations with multiyear data sets, modeling will be used as an integrative tool to investigate the question of how climate change and anthropogenic activities could impact the cycle of biogenic elements and marine ecosystems.

The present study aims to quantify the dynamics of nutrients at the seasonal scale and to estimate an annual budget of nitrogen and phosphorus, in the NW Med dense water formation area. After a brief description of the observation network, the modeling strategy is described (section 2), and then evaluated through comparisons with observations (section 3). The seasonal variabilities of the atmospheric forcing and hydrography are presented (section 4.1.1), together with the annual cycles of nutrient stocks in the upper layer (section 4.1.2). In section 4.1.3, we discuss the impact of physical and biogeochemical processes on the N:P ratio in the upper layer. Finally, an annual nitrogen and phosphorus budget of the region is proposed (section 4.2).

2. Method

2.1. Observations

During the period from September 2012 to September 2013, a large number of hydrological and biogeochemical observations (>178 profiles) were made in the NW Med in the framework of the MERMEX (Marine Ecosystems Response in the Mediterranean Experiment) and HyMeX (Hydrological cycle in the Mediterranean Experiment) programs. The objective was to better understand the interactions between horizontal and vertical physical processes during a convection event (Estournel et al., 2016a) and their impact on nutrient budgets and marine ecosystems.

In this study, we used the observations collected during three cruises that covered the NW Med in winter, spring and summer of 2013. During DeWEX Leg 1, conducted from 1 to 21 February 2013 on board the R/V Le Suroit, 75 hydrological and 45 biogeochemical profiles were obtained (Figure 1b; Severin et al., 2017; Testor, 2013), with the objective of globally mapping the convection area, the distribution of the newly formed deep waters and the distribution of inorganic and organic matter. DeWEX Leg 2 sampled the spring bloom from 5 to 24 April 2013 (Conan, 2013; Mayot et al., 2017). It followed the same sampling network as the winter cruise, with 99 hydrological profiles and 59 biogeochemical profiles (Figure 1c; Severin et al., 2017). The third cruise was carried out during the oligotrophic period, between 24 July and 7 August 2013, in the framework of the integrated observation network MOOSE (Mediterranean Ocean Observing System for the Environment; Testor et al., 2013). One hundred biogeochemical profiles were measured (Figure 1d).

Then, data provided by the Bio-Argo float LovBio17b between April and September 2013 (Pasqueron de Fommervault et al., 2015b) were used to assess the modeled vertical evolution of the nitrate concentration. LovBio17b provided 73 vertical profiles at a daily frequency during the first 55 days of spring, and then at 5 day frequency for the next summer weeks. Calibration was performed at the deployment using in situ observations from 0 to 1,000 m depth (about 10 m resolution in the 0–250 m layer, and 30 m below).

2.2. Modeling

2.2.1. Hydrodynamics

The SYMPHONIE model used in this study is a 3-D primitive equation, with free surface and generalized sigma vertical coordinate, described by Marsaleix et al. (2008, 2009, 2011, 2012). It was previously used for the Mediterranean Sea to simulate convection in the deep sea (Estournel et al., 2016b; Herrmann et al., 2008), coastal dense water formation (Estournel et al., 2005; Ulses et al., 2008), and circulation on the continental shelf of the Gulf of Lions (Petrenko et al., 2008). The numerical domain (Figure 1a) covers most of the western Mediterranean basin, using a curvilinear grid with variable horizontal resolution (Bentsen et al., 1999). The resolution is 1.4 km to the south and about 0.8 km to the north. The southward decrease of the resolution is intended to cover the W Med basin at a more reasonable cost while considering the northward decrease of the Rossby radius, in particular the need for increased resolution in the winter dense water formation area (Estournel et al., 2016b).

Forty vertical levels were used with closer spacing near the surface (15 levels in the first 100 m in the center of the convection zone characterized by depths of $\sim 2,500$ m). The model was initialized and forced at its lateral boundaries with daily analyses provided by the Mercator-Ocean operational system based on the NEMO ocean model (Maraldi et al., 2013). The configuration of this model was the PSY2V2R4 prototype based on the NEMO Ocean modeling platform and the SAM data assimilation system (Lellouche et al., 2013) at a resolution of $1/12^\circ$ over the Atlantic and the Mediterranean from 20°S to 80°N . As in Estournel et al. (2016b), the initial field and open boundary conditions were corrected for stratification biases deduced from comparisons between analysis and observations taken during the MOOSE cruise of August 2012. The atmospheric forcing (turbulent fluxes) was calculated using the bulk formulae of Large and Yeager (2004). Meteorological parameters, including radiative fluxes, were given by the ECMWF operational forecasts at $1/8^\circ$ horizontal resolution and 3 h temporal resolution based on daily analysis at 00.00 UTC. Since the underestimation of strong winds is a source of uncertainty in atmospheric forcing (Herrmann et al., 2010), Estournel et al. (2016b) performed sensitivity tests to the wind speed. According to those tests, the wind velocity was increased by 13% in order to increase the accuracy of the model results in reproducing the convection event (Estournel et al., 2016b) in our hydrodynamic simulation. River runoffs were considered using measured daily values for French rivers (data provided by Banque Hydro, www.hydro.eaufrance.fr) and the Ebro (data provided by SAIH Ebro, www.saihebro.com) and mean annual values for the others.

2.2.2. Biogeochemistry

The Eco3M-5 model (Ulses et al., 2016) is a multnutrient and multiplankton functional type model that simulates the dynamics of the biogeochemical decoupled cycles of several biogenic elements (carbon, nitrogen, phosphorus, silicon, and oxygen) and of non-Redfieldian plankton groups. The model comprises seven compartments. A first compartment of phytoplankton classified by size is described by the mechanistic formulations of the model Eco3M (Baklouti et al., 2006), where picophytoplankton ($0.7\text{--}2\ \mu\text{m}$) and nanophytoplankton ($2\text{--}20\ \mu\text{m}$) are composed of dinoflagellates, and microphytoplankton ($20\text{--}200\ \mu\text{m}$) is composed of diatoms. A second compartment of zooplankton is composed of nanozooplankton ($5\text{--}20\ \mu\text{m}$; small flagellates), microzooplankton ($20\text{--}200\ \mu\text{m}$; ciliates and large flagellates) and mesozooplankton ($>200\ \mu\text{m}$; copepods and amphipods). A third compartment, bacteria, is also considered. The behavior of heterotrophic organisms is derived from the model by Anderson and Pondaven (2003). The other compartments are dissolved organic matter, particulate organic matter (small and large, differentiated by the settling speed and origin), inorganic nutrients (nitrate, ammonium, phosphate, and silicate) and dissolved oxygen. A total of 34 state variables are calculated. The model structure (Figure 2) used in this study is based on the same pelagic plankton ecosystem model as the one fully described and used by Auger et al. (2011) and Ulses et al. (2016). Here we recall the equations of the rates of change of the nitrate and phosphate, since we will discuss the time evolution of their stock and of their ratios in section 4.1:

$$\frac{\partial[\text{NO}_3]}{\partial t} = \text{Nitrification} - \text{PhytoplanktonUptake}, \quad (1)$$

$$\frac{\partial[\text{PO}_4]}{\partial t} = \text{ZooplanktonExcretion} + \text{BacteriaExcretion} - \text{PhytoplanktonUptake}, \quad (2)$$

where *Nitrification* is the nitrification rate, *PhytoplanktonUptake* is the nutrient uptake by phytoplankton, and *ZooplanktonExcretion* and *BacteriaExcretion* are the nutrient excretions by zooplankton and bacteria,

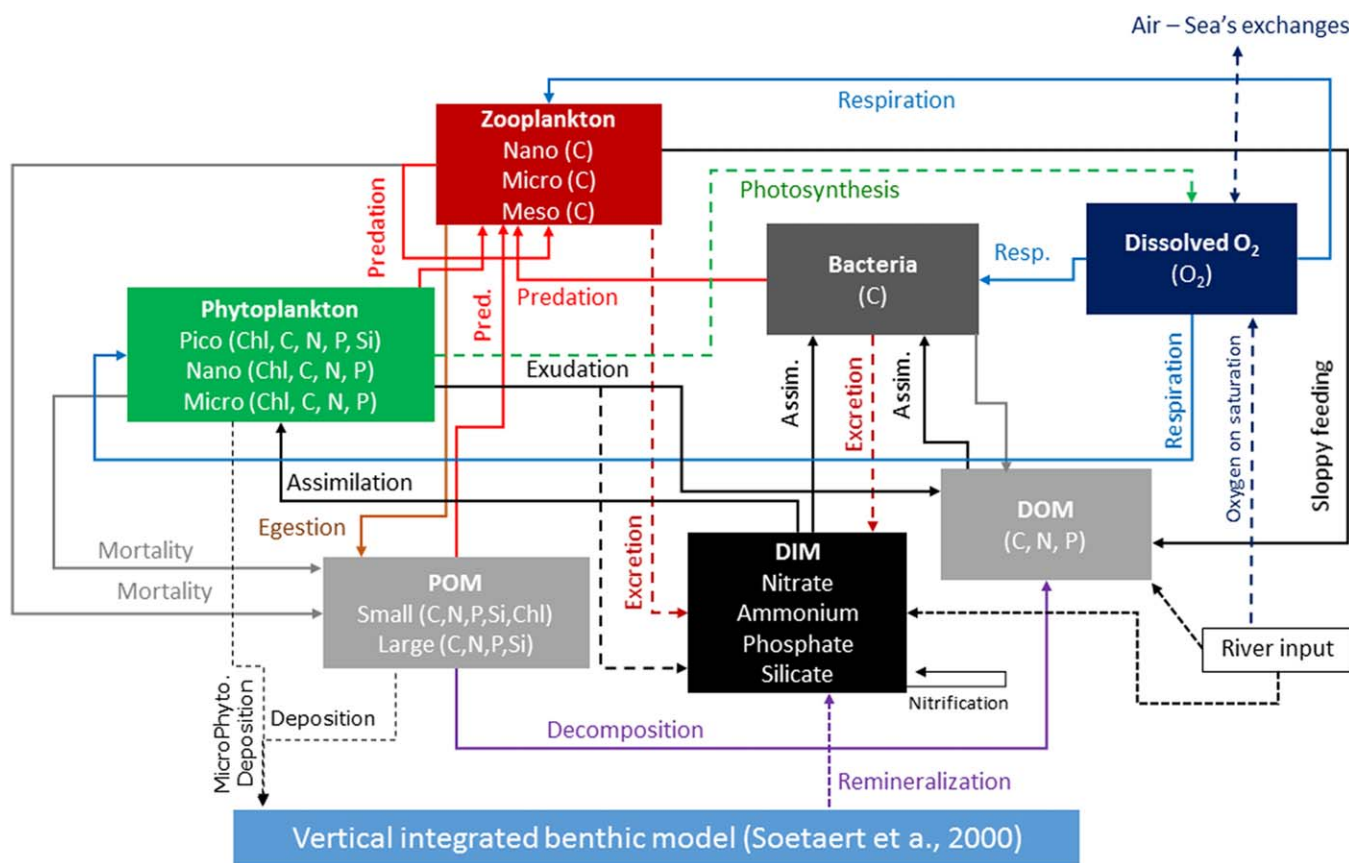


Figure 2. Eco3M-S biogeochemical model scheme.

respectively. The formulas of these fluxes are given in Auger et al. (2011, their Table A.4). The uptake of nutrients by phytoplankton (*PhytoplanktonUptake*) depends on the gross primary production rate and on the nutrient concentrations (Auger et al., 2011, A19–A22 in Table A.4). Excretions (*ZooplanktonExcretion* and *BacteriaExcretion*) are the processes enabling heterotrophs to keep their internal composition constant by releasing the excess elements in the form of dissolved inorganic matter (Auger et al., 2011, A38–A42 in Table A.4). *Nitrification* is the production of nitrate by bacteria, represented here in an implicit way by a first order function of the ammonium concentration (Auger et al., 2011, A55 in Table A.4). *Nitrification* is regulated by light intensity and temperature. For the present study of the NW Med, where winter convection favors strong vertical transport of nutrients in the photic zone, we neglected the process of nitrogen fixation. This process has been shown to have only a small effect on stoichiometry in the W Med (Ribera d'Alcalà et al., 2003). Most of the values of biogeochemical model parameters were based on the previous modeling study by Ulses et al. (2016), but some parameters were recalibrated using several data sets (MODIS, BOUM, MOOSE-GE, and DeWEX cruises).

In this study, we used the “Source Splitting” coupling method (Butenschön et al., 2012). It consists in an off-line forcing of the biogeochemical model by the daily averaged outputs of the physical model. A time step of a few minutes was used for the advection and diffusion of biogeochemical variables, while Eco3M-S computed the biogeochemical fluxes with a time step of about 1 h. It was then assumed that biogeochemical properties do not significantly impact the hydrodynamics.

The biogeochemical model was downscaled from the Mediterranean basin scale to the regional scale as described hereafter. First, the biogeochemical basin scale model was forced by the daily fields from the NEMO model (PSY2V2R4 analyses), also used for the boundary conditions of the hydrodynamic model as indicated in section 2.2.1. This basin configuration was initialized in June 2010 with climatological nutrient fields from the Medar/MedAtlas database (Manca et al., 2004) corresponding to oligotrophic conditions. Daily values of all state variables were extracted from the basin run for the initial and lateral boundary

conditions of the regional model. This nesting protocol ensures coherence of the physical and biogeochemical fields at the open boundaries. The regional model was initialized in August 2012.

At the mouth of the Rhone River, nitrate, ammonium, phosphate, silicate, and dissolved organic carbon concentrations were prescribed using in situ daily data (P. Raimbault, personal communication, 2015). Concentrations of dissolved organic phosphorus and nitrogen and also of particulate organic matter were estimated from these data and the relations deduced from the literature (Moutin et al., 1998; Sempéré et al., 2000) as described in Auger et al. (2011). At the other river mouths, climatological values were prescribed according to Ludwig et al. (2010). The deposition of organic and inorganic matter from the atmosphere was neglected in this study. The benthic fluxes of inorganic nutrients were considered by coupling the pelagic model with a simplified version of the meta-model described by Soetaert et al. (2001). The parameters of this model were set according to the modeling study on the Gulf of Lions shelf performed by Pastor et al. (2011).

2.3. Area of Study

The analysis of the nitrogen and phosphorus seasonal cycles, and annual budgets, was performed for the deep convection area of the NW Med, defined here using a mixed layer criterion. This region (indicated in blue in Figure 1a), named deep convection area (DCA) hereafter, represents the area where the mixed layer depth (MLD), defined in section 2.4, exceeded 1,000 m for at least 1 day during the study period. According to the model, it covered more than 61,700 km² in 2013.

For the analysis and budget estimates, we divided the water column into two layers: an upper layer corresponding to the layer where primary production takes place and a deep layer corresponding to the reservoir of inorganic nutrients. We chose to delimit these two layers with a nutricline criterion. The depth of the nutricline varies over time. As a variable depth would not allow a simple analysis of stock variations and annual budget of processes, we took a constant value corresponding to the maximum depth of the nutricline in the model domain, equal to 130 m, as our criterion. As the gradient of nutrient concentration is strong at the nutricline depth, the model estimate of nutrient stock in the upper layer is highly sensitive to the depth criterion. For instance, an overestimation of the nutricline depth in the model would lead to an underestimation of the modeled nutrient stock. In this study, we focus then on the variation of the nutrient inventory rather than on the value of this inventory. Moreover, we consider the temporal variation of nutricline depth when analyzing that of upper layer nutrient stock.

Besides, previous studies (Körtzinger et al., 2008; Martin & Pondaven, 2006) demonstrated that material exported below the productive layer could be resuspended within this zone during mixing periods. Then the maximum yearly mixed layer depth was recommended as a threshold to calculate the export flux or new primary production (Martin & Pondaven, 2006; Palevsky et al., 2016). The computation of the modeled export of organic and inorganic matter as the sum of sedimentation (for particulate matter) and net flux induced by turbulent mixing and vertical advection in the present study avoids counting the export of organic and inorganic matter that is then reinjected into the upper layer during mixing periods. However, we are aware that if new primary production is considered as the algal growth fueled by nitrate coming in the upper layer for the first time of the studied year, then it could be overestimated due to the recycling of exported organic material in the deep layer whose products would be upwelled back in the upper layer during the mixing period. The estimate of nitrification in the upper layer will be used to estimate this overestimation.

2.4. Derived Variables

Variables used for the analysis of the annual cycles and budgets were derived from the coupled model. The modeled MLD is defined as the depth where the potential density exceeds its value at 10 m below the surface by 0.01 kg m⁻³. We calculated the depths of the 1 mmol N m⁻³ and 0.05 mmol P m⁻³ isoconcentrations of nitrate and phosphate, as a proxy of the depths of the nitracline and phosphacline, respectively, according to Lavigne (2013) and Lazzari et al. (2012) studies. Both depths are significantly correlated in time in this region ($R = 0.84$, $p < 0.01$) and the maximum difference between the depths of the nutriclines is 10 m. For this reason, the nutricline refers to both the nitracline and the phosphacline hereafter. The stock of nutrients in the surface layer (0–130 m) was calculated in the simulation. Moreover, we computed a second estimate of the nutrient stock in the deep convection area using the observations from

the three cruises described in section 2.1. The nutrient concentrations measured during the cruises were interpolated over the model grid and then integrated in the 0–130 m layer as in the model. The interpolation method considers not only the notion of distance in space but also the deviation from selected physical fields (temperature and salinity). In practice, the nitrate and phosphate fields are interpolated from the cruise data (74 vertical nutrient profiles for MOOSE, 104 nutrient profiles for DEWEX cruises). It is therefore possible to estimate the deviation of temperature and salinity between all points of the numerical grid and the points corresponding to the position of the nutrient profiles to be interpolated. Since the bathymetry of a region such as the Mediterranean has a great influence on the organization of the circulation, the bathymetry deviation was also considered in a similar way. Finally, the concentration of the nutrients C at grid point (x, y, z) was obtained in the following way:

$$C(x, y, z) = \frac{\sum_q W_q C(q, z)}{\sum_q W_q}, \quad (3)$$

where q is the nutrient profile number, $C(q, z)$ the concentration of nutrients at the point corresponding to the position of the nutrient profile q and depth z , and W_q the weight depending on the tracers and bathymetry deviations according to

$$w_q = e^{-\left(\frac{S_{x,y,z} - S_{q,z}}{\delta S_0}\right)^2} \times e^{-\left(\frac{T_{x,y,z} - T_{q,z}}{\delta T_0}\right)^2} \times e^{-\left(\frac{H_{x,y} - H_q}{\delta H_0}\right)^2} \times e^{-\left(\frac{D_q}{D_0}\right)^2}, \quad (4)$$

where $S_{x,y,z}$ is the salinity, and δS_0 is an empirically determined scale of salinity variation (the terms related to temperature $(T_{x,y,z})$ and bathymetry $(H_{x,y})$ are obtained in a similar manner), D_q is the horizontal distance between the considered grid point and the nutrient profile q , D_0 is an empirically determined scale of distance.

Finally, we deduced a value of the N:P ratio from the ratio of nitrate to phosphate stocks in the upper layer, INO_3 and IPO_4 (in mmol m^{-2}), respectively. The contribution of biogeochemical or physical processes to the change of N:P ratio, was computed with equation (5):

$$\frac{\partial(N : P)}{\partial t} = \frac{IPO_4 \frac{\partial INO_3}{\partial t} - INO_3 \frac{\partial IPO_4}{\partial t}}{(IPO_4)^2},$$

where $\frac{\partial INO_3}{\partial t}$ and $\frac{\partial IPO_4}{\partial t}$ (in $\text{mmol m}^{-2} \text{d}^{-1}$) are the rates of change of upper layer nitrate and phosphate stocks, respectively:

$$\frac{\partial INO_3}{\partial t} = \text{VertNO}_3 + \text{HorAdvNO}_3 + I\left(\frac{\partial[NO_3]}{\partial t}\right)_{\text{bio}}, \quad (6)$$

$$\frac{\partial IPO_4}{\partial t} = \text{VertPO}_4 + \text{HorAdvPO}_4 + I\left(\frac{\partial[PO_4]}{\partial t}\right)_{\text{bio}}, \quad (7)$$

where VertNO_3 and VertPO_4 are the net upward fluxes of nitrate and phosphate, respectively, at 130 m depth, due to vertical advection and turbulent mixing, HorAdvNO_3 and HorAdvPO_4 are the net horizontally advected inputs of nitrate and phosphate, respectively, in the upper layer from surrounding regions, $I\left(\frac{\partial[NO_3]}{\partial t}\right)_{\text{bio}}$ and $I\left(\frac{\partial[PO_4]}{\partial t}\right)_{\text{bio}}$ are the upper layer integrated biogeochemical processes (see equations (1) and (2)).

2.5. Statistical Analysis of the Model Results

A point-to-point approach was used to quantify the performance of the model in its ability to represent the dynamics of inorganic nutrients and chlorophyll over the study period. The model results were compared with the observations at the same dates and positions. Following the recommendations of Allen et al. (2007), we calculated four metrics: the standard deviation ratio ($r_\sigma = \frac{\sigma_m}{\sigma_o}$ where σ_m and σ_o are the standard deviation of model outputs and observations, respectively); the Pearson correlation coefficient ($R = \frac{1}{K} \frac{\sum_{n=1}^K (m_n - \bar{m})(o_n - \bar{o})}{\sigma_m \times \sigma_o}$), where K is the number of observations, m_n is the model output that corresponds to the observation n , o_n , \bar{m} , and \bar{o} are the mean of model outputs and observations, respectively); the Nash-Sutcliffe efficiency ($NS = 1 - \frac{\sum_{n=1}^K (o_n - m_n)^2}{\sum_{n=1}^K (o_n - \bar{o})^2}$) and the percentage bias ($PB = \frac{\bar{m} - \bar{o}}{\bar{o}}$). The calculation of these

four-complementary metrics enabled different aspects of the model results to be assessed. The standard deviation ratio assessed the variability in the model results compared to that in observations, a value of $r_{\sigma} > 1$ indicating that the variability was stronger in the model outputs than in observations. The correlation coefficient assessed the similarity between model and observations and significant correlations ($p < 0.01$) were obtained for all R calculations presented in section 3. The Nash-Sutcliffe efficiency assessed the difference between model and observations compared to the variability in the observations. According to Allen et al. (2007), a value >0.65 indicates excellent performance, (0.65, 0.5) is very good, (0.5, 0.2) is good, and <0.2 indicates poor performance. Finally, the percentage bias indicated a general overestimation in the model results when it was positive and conversely. According to Allen et al. (2007), the performance of the model can be considered as excellent if the percentage bias is $<10\%$.

3. Comparison of Model Results With Observations

An evaluation of the hydrodynamic simulation is described in Estournel et al. (2016b) where modeled temperature and salinity were compared with different available sets of observations. The present study focuses on evaluating the model's ability to reproduce the spatial and temporal variability of inorganic nutrients.

3.1. Comparison With Winter, Spring, and Summer Cruise Observations

To evaluate the model's performance to reproduce the horizontal and vertical biogeochemical patterns in relation with the hydrology, the simulation was compared to the observations from cruises that took place during three key periods for the ecosystem (winter, spring, and summer). For winter and spring periods, first, we compared the surface concentrations of nutrients. Then the model/observations comparison was made over the water column along a transect across the deep convection area, from the Balearic Islands to the Gulf of Lions shelf (measurement locations are indicated by the red dots in Figure 1b for winter and Figure 1c for spring). For both comparisons, the modeled concentrations of nutrients were averaged over the period of sampling: 21 and 20 days for the surface observations, and 2 and 3 days for the transect observations, for the winter and spring cruises, respectively.

3.1.1. Winter

In winter, during the winter cruise, modeled and observed surface concentrations of nitrate and phosphate (Figures 3a and 3b) show some heterogeneity. The model indicates that the patch of high surface nutrient concentrations ($>7.5 \text{ mmol m}^{-3}$ for nitrate and $>0.3 \text{ mmol m}^{-3}$ for phosphate) was located between 40.5°N and 43°N and between 3°E and 8°E . These characteristics and values match the observations, which show surface concentrations $>7.64 \text{ mmol m}^{-3}$ for nitrate and $>0.35 \text{ mmol m}^{-3}$ for phosphate (Severin et al., 2017). The highest values corresponded to the center of the deep convection region where intense convection brought nutrients to the surface layer (Severin et al., 2017). Outside the convective mixed patch, the surface nutrient concentrations were very low ($<1 \text{ mmol m}^{-3}$ for nitrate and $<0.05 \text{ mmol m}^{-3}$ for phosphate) as detected in the observations south of latitude 41°N . Between these two regions, a strong gradient was observed and modeled on a narrow band. Around the convective patch, in the Balearic Sea and in the Gulf of Lions, the observations show values close to 2.95 mmol m^{-3} for nitrate and 0.11 mmol m^{-3} for phosphate, while the model overestimates these values by 1 mmol m^{-3} for nitrate and by 0.4 mmol m^{-3} for phosphate. The strong gradient between the deep convection patch and the surrounding areas was a location of complex frontal dynamics. The greatest biases could originate from vertical motions at very fine scale on these fronts. Nevertheless, it is interesting to note the fine scale structures in the model, which could be explained by the enrichment of deep nutrients induced by the small-scale dynamics.

Figures 3c–3e give complementary information on the vertical distribution of chlorophyll and nutrient concentrations in the model compared with the observations. Between latitudes 41.5°N and 42.5°N , the modeled and observed water column was homogeneous in biogeochemical variables. Both model and observations show that the surface chlorophyll a concentration was minimum in the deep convection area (lower than 0.10 mg m^{-3} in the model, lower than 0.16 mg m^{-3} in the observations). This feature was previously highlighted using satellite data and 3-D coupled modeling (Auger et al., 2014; Herrmann et al., 2017; Houpert et al., 2016) and was explained by a low phytoplankton growth and/or the vertical dilution of phytoplankton cells throughout the whole mixed layer that can reach the ocean bottom ($\sim 2,500 \text{ m}$). The maximum vertical gradient of nutrients corresponded to the 29.05 kg m^{-3} isopycnal (superimposed on vertical sections; Figures 3c–3e) at the northern and southern limits of the deep convection area. The isopycnal

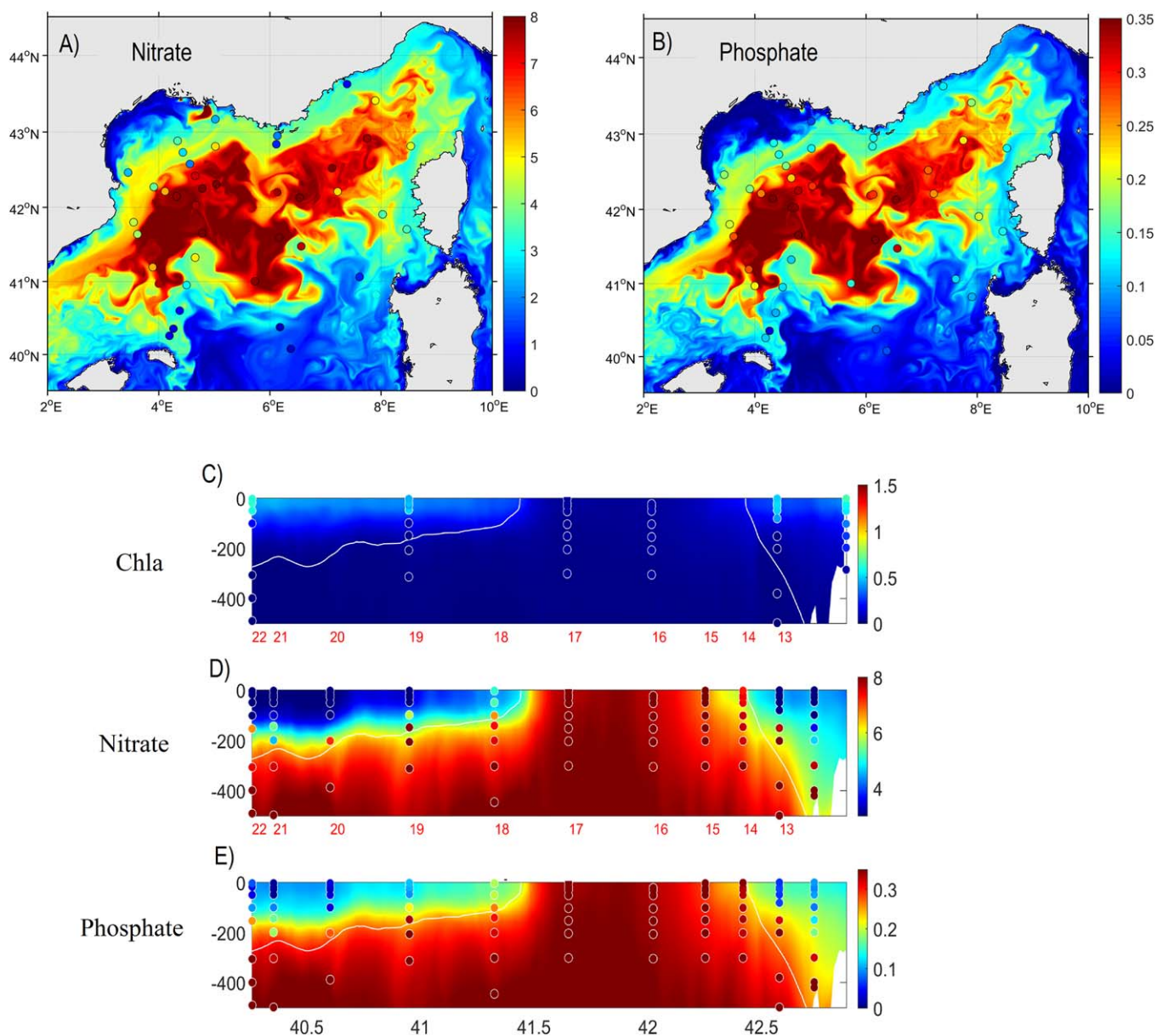


Figure 3. Comparison of modeled and observed surface (a) nitrate and (b) phosphate concentrations (mmol m^{-3}) during the winter cruise. Vertical section of (c) chlorophyll (mg m^{-3}), (d) nitrate (mmol m^{-3}), and (e) phosphate (mmol m^{-3}) concentrations across the deep convection area, indicated by red dots in Figure 1b. The model is represented by background colors and observations are indicated in colored circles (DeWEX Leg1, February 2013). White lines in the vertical sections (Figures 3c–3e) represent the 29.05 kg m^{-3} isopycnal potential density anomaly. The maps (Figures 3a and 3b) correspond to an average modeled concentration over the period of the cruise (1–21 February) while the vertical cross section represents a model average over the transect observation period (12–13 February). The numbers of the measurement stations along the vertical section are indicated in the x axis of Figures 3c and 3d. Latitudes are indicated in the x axis of Figure 3e.

depth varies between 200 m to the south and 400 m to the north. Beyond this threshold, modeled nitrate concentration increased from 6 to 8 mmol m^{-3} and phosphate concentration from 0.2 to 0.35 mmol m^{-3} .

Vertical homogeneity, at least over several hundred meters in the center of the deep convection area, in temperature, salinity (Estournel et al., 2016b), and nutrient concentrations, was also observed during winter 2011 as reported by Severin et al. (2014) and D'Ortenzio et al. (2014). Other authors (Dilek et al., 2005; Gačić et al., 2002; Santinelli et al., 2012; Yilmaz & Tugrul, 1998) have reported some homogeneous biogeochemical profiles and high surface inorganic matter enrichment by convective mixing in the eastern Mediterranean basin as mentioned before.

When comparing modeled nitrate and phosphate concentrations (mean values and standard deviations: 6.35 ± 1.92 and 0.26 ± 0.09 mmol m⁻³), respectively, with the whole winter cruise observations (mean values and standard deviations: 6.45 ± 2.66 and 0.28 ± 0.13 mmol m⁻³), we find a Pearson correlation coefficient of 0.87 and 0.89 (p -value < 0.01), respectively, and a Nash-Sutcliffe efficiency of 0.73 and 0.75, respectively, both indicating excellent performance of the coupled simulation. The standard deviation ratio of 0.72 and 0.73, for nitrate and phosphate concentrations, respectively, indicates a lower variability in model results than in observations, and the percentage biases of -1.5% and -5.5%, respectively, an underestimation of nutrient concentrations, visible around the convective region in Figure 3. Regarding the modeled chlorophyll concentrations (mean value and standard deviation: 0.12 ± 0.16 mg m⁻³) compared to that observed on the cruise period (mean value and standard deviation: 0.18 ± 0.19 mg m⁻³), the Pearson coefficient correlation of 0.81 and the Nash-Sutcliffe efficiency of 0.56 show that the model reproduces very well the spatial phytoplankton distribution. However, the percentage bias shows that the model underestimates the observations by 32% in average.

3.1.2. Spring

In spring, nutrient and chlorophyll patterns (Figure 4) changed drastically compared to February 2013. Severin et al. (2017) attributed these changes to a strong phytoplankton development that was considered as a bloom by Mayot et al. (2017). In this study, the onset of the bloom was considered as the day when the net accumulation rate of the carbon biomass integrated through the water column (Behrenfeld, 2010) exceeded 50% of its maximum yearly value. Surface nutrient concentrations were low (Figures 4a and 4b) but remained higher in the deep convection area than outside. In the observations, as in the model, surface values of 2–3 mmol m⁻³ of nitrate and 0.08–0.12 mmol m⁻³ of phosphate were observed in the center of the basin, while oligotrophic conditions were becoming established outside the deep convection area, with surface nutrient concentrations down to 0 mmol m⁻³ in some areas away from the convection zone. In general, the model appears to underestimate the surface nutrient concentrations.

Figures 4d and 4e give an estimation of the nutricline depth, located at 60 m in average (standard deviation: 20 m) in the model, and following the density gradient. A surface chlorophyll development was observed and modeled (Figure 4c) in conjunction with the nutrient depletion (Figures 4d and 4e), with a concentration exceeding 1.5 mg m⁻³ in the first 30 m, then 0.4 ± 0.2 mg m⁻³ from 30 to 60 m and zero below 60 m. A homogeneous physical, biogeochemical profile was observed at the station 42°N, 5°E in 8 April. Although the model reproduces this homogeneous feature, the modeled nutrient concentrations are underestimated and the chlorophyll concentration is overestimated in the surface layer at this station (not shown on the 3 days average in Figures 4c–4e). The model simulates during April, several short wind gust events that interrupted the bloom development and mixed the upper layer. The strong gusts of wind associated with negative heat flux that occurred on 6 and 19 April are examples, visible in Figure 7. These events resulted in a temporary decrease of the chlorophyll surface concentrations, and an increase of nutrients in mesoscale structures. Restratification followed the wind events, and reconstructed the bloom conditions. The comparisons of model results with observations suggest that the location of these mesoscale structures is not correctly reproduced in the model.

The calculation of metrics indicates that the model reproduces very well the spatial distribution of the whole nitrate and phosphate concentrations observed during the spring cruise (mean values and standard deviations in the model: 5.07 ± 2.92 and 0.21 ± 0.13 mmol m⁻³, respectively, mean values and standard deviations in observations: 5.44 ± 3.09 and 0.23 ± 0.14 mmol m⁻³, respectively): the correlation coefficients are 0.91 and 0.90 (p -value < 0.01), respectively, the Nash-Sutcliffe efficiencies are 0.80 and 0.77, respectively. The model presents lower variability by 5 and 6% and underestimates by 6 and 8% the nitrate and phosphate concentrations, respectively. Regarding the chlorophyll concentrations (mean value and standard deviation in the model: 0.38 ± 0.45 mg m⁻³, mean value and standard deviation in observations: 0.56 ± 0.79 mg m⁻³), a good correlation (0.77) and a good Nash-Sutcliffe efficiency (0.50) between model and observations are found. The percentage bias indicates that the model underestimates observed chlorophyll concentration by 32%.

3.1.3. Summer

Comparisons of modeled nitrate and phosphate concentrations in summer conditions (mean values and standard deviations: 6.24 ± 3.10 and 0.15 ± 0.25 mmol m⁻³, respectively) with the whole summer cruise observations (mean values and standard deviations: 5.02 ± 3.28 and 0.15 ± 0.19 mmol m⁻³, respectively), at the same dates and locations, are shown in Figure 5. From the bottom to 300 m depth, the modeled nutrient concentrations fall in the observed range. However, one can notice that most of the modeled nutrient

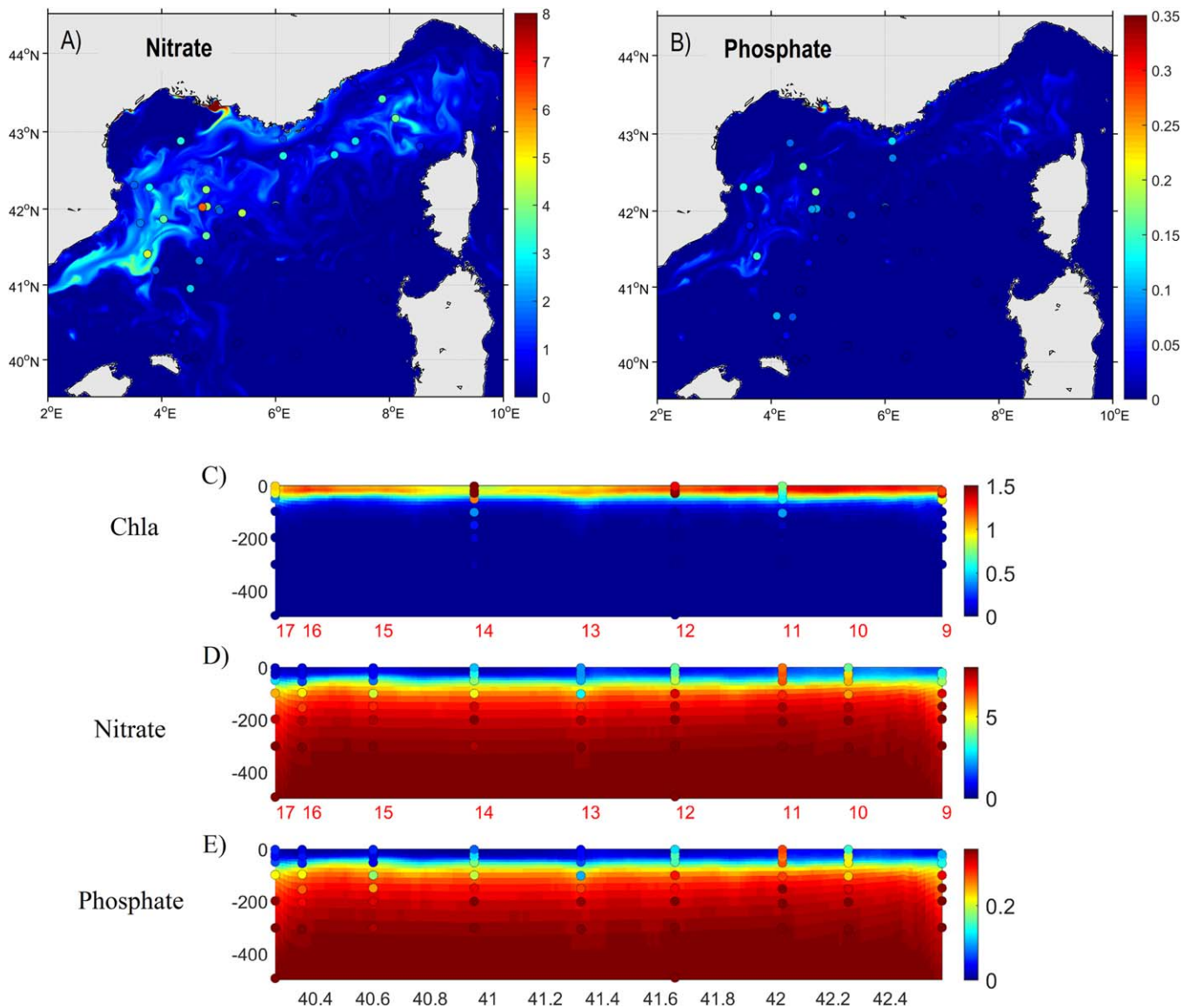


Figure 4. Same as Figure 3 but for spring cruise (DeWEX Leg 2) in April 2013. Model outputs are averaged (a, b) over the period 5–24 April and (c–e) over the period 8–10 April. The numbers of the measurement stations along the vertical section are indicated in the x axis of Figures 4c and 4d. Latitudes are indicated in the x axis of Figure 4e.

concentrations in deep layers are in the upper range of the observed profiles. The nutrient gradient at 100 m depth is well reproduced by the model. However, higher values of modeled phosphate are visible at 50, 150, and 200 m depth. The model reproduces then correctly the depletion of nutrients in the 0–50 m surface layer.

We find a Pearson correlation coefficient of 0.82 and 0.82 (p -value < 0.01), and a Nash-Sutcliffe efficiency of 0.52 and 0.46, for nitrate and phosphate concentrations, respectively, both metrics indicating excellent performance of the coupled simulation. The standard deviation ratio of 0.94 and 1.04, for nitrate and phosphate concentrations, respectively, indicates small differences in the variability in model results compared to observations, and the percentage bias of 24% and 32%, respectively, an overestimation of nutrient concentrations in the model.

3.2. Variability Between April and September 2013

The objective of this section is to evaluate the ability of the model to reproduce the variability of the biogeochemistry during a transitional phase. The Bio-Argo float Lovbio17B deployed in the NW Med in April

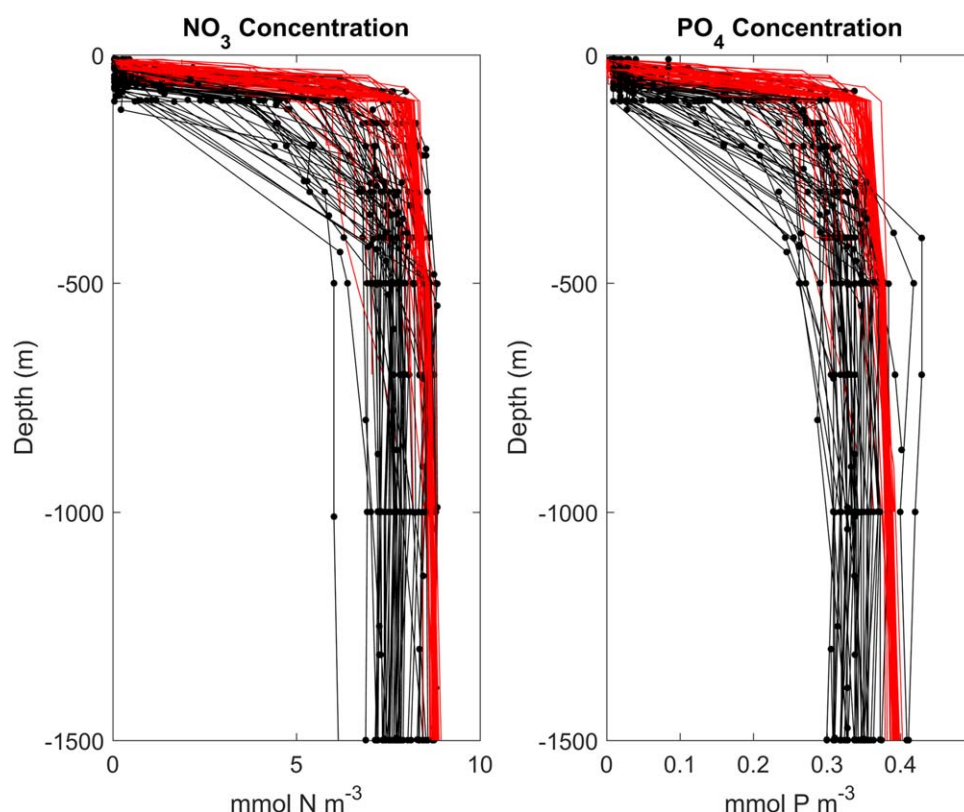


Figure 5. Comparison of modeled (red) and observed (black) nitrate and phosphate concentration (mmol m^{-3}) profiles during MOOSE cruise in July 2013.

2013 during the bloom presents a time series of the nitrate concentration that describes the transition in the surface layer from the bloom to the oligotrophic phase.

Figure 6 shows an evolution of nitrate concentration measured by the float and simulated by the model at the same points. The deepening of the nitracline occurs earlier in the model than in the observations. The nitrate concentration measured by the float in April is 1 mmol m^{-3} higher than in the model but measured and modeled concentrations are identical in May, with a nutricline located at the same depth ($\sim 50 \text{ m}$). Variations of nitrate concentrations from 0 to 7 mmol m^{-3} in less than 30 m were observed in the surface layer and were correlated to high frequency motions distinctly detected in both observations and model in April and May. These motions seem to supply nutrients into the mixed layer (the depth of which is indicated by the green dashed line in Figure 6) more efficiently in the observations. This could be explained by an underestimation of the vertical gradient at 100 m in the model, as shown also in Figures 4d and 4e. However, in the model results and observations, after each pulse of nutrient injection, the nitrate depletion in the surface layer was fast and the nutricline deepened with time from 50 m at the beginning of June to 70 m during the whole summer. At the same time, a shallow mixed layer was observed around 10–15 m.

The calculated metrics show that the model can correctly reproduce the transitional phase observed by the float. The Pearson correlation coefficient ($R = 0.94$) and the Nash-Sutcliffe efficiency ($NS = 0.82$) indicate excellent performance of the model. However, slightly higher variability in the observation is indicated by the standard deviation ratio of 0.95. The float measured concentrations higher than 1 mmol m^{-3} in the upper layer from May to October, when the model's concentrations were very low above the nitracline. A general underestimation by the model is indicated by the percentage bias of -16% .

4. Results and Discussion

The comparison exercise reveals that the coupled model is able to reproduce the general seasonal dynamics of inorganic nutrients and phytoplankton growth deduced from the cruise observations. The spatial

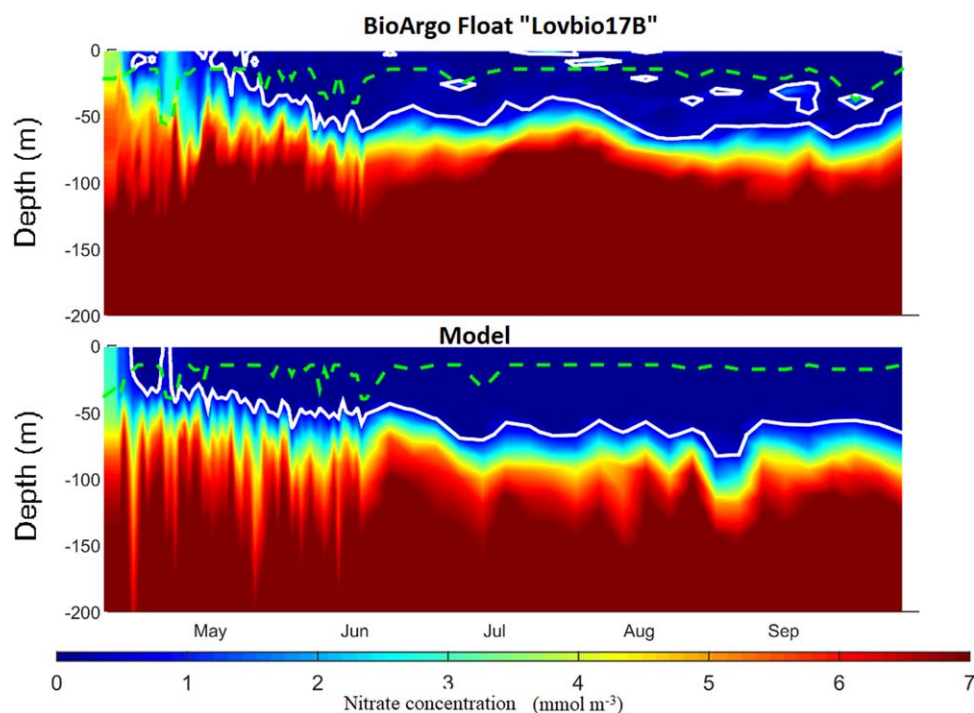


Figure 6. Hovmöller diagram of the nitrate concentration (mmol m^{-3}) along the float track from April to September 2013. Data are extracted (top) from the float Lovbio17B and (bottom) from the model. White line represents the depth of the nitracline (position of the 1 mmol m^{-3} concentration) and the green dashed line represents the MLD.

extension of the convection area, where deep inorganic nutrients were upwelled and phytoplankton were diluted over the whole water column, appears to be in good agreement with cruise observations. The model reproduces the strong inorganic nutrient decrease between winter and spring cruises. Finally, the modeled depletion of nutrients of the upper layer in summer agrees with MOOSE and Lovbio17B observations. However, the model appears to generally underestimate the observed surface nutrient concentrations in spring and to anticipate the deepening of the nutricline observed by the Bio-Argo float.

Aware of the weaknesses and the strengths of the present coupled simulation, in the following sections, we use the model outputs to disentangle the impact of the physical and biogeochemical processes on the seasonal variations of the nutrient stock and stoichiometry in the upper layer of the deep convection area, from September 2012 to September 2013. Finally, the model is also used to estimate a budget of nitrogen and phosphorus in the upper and deeper layers over the 1 year study period.

4.1. Annual Cycle of Nutrients

4.1.1. Atmospheric Forcing and Ocean Vertical Mixing

Figure 7 presents the time series of the modeled heat flux at the LION station (42°N , 5°E), located in the center of the deep convection area, and Figure 8 presents the time series of the modeled MLD averaged over the deep convection area, from September 2012 to September 2013. Seasonal variability of the atmospheric forcing is clearly visible. In September and October 2012, positive heat fluxes were regularly interrupted by short, strong heat loss events corresponding to wind gusts from the north. In late October, an extreme heat loss event ($-1,300 \text{ W m}^{-2}$) severely weakened the stratification of the upper layer and the spatially averaged MLD deepened by 20 m (Figure 8). In late November/early December, a strong wind episode lasted three weeks. Then a succession of heat loss events followed from mid-January to the end of February. From December, each event produced a pronounced increase of the MLD. At the beginning of February, the ML reached the seafloor in the deep convection center (not shown), when the spatially averaged MLD reached 1,500 m (maximum deepening not shown in Figure 8). A final short, strong wind episode occurred between the second and the third weeks of March. This event caused a breakdown of the weak restratification established during the calm second week of March. Winter 2013 was thus characterized by a first and main

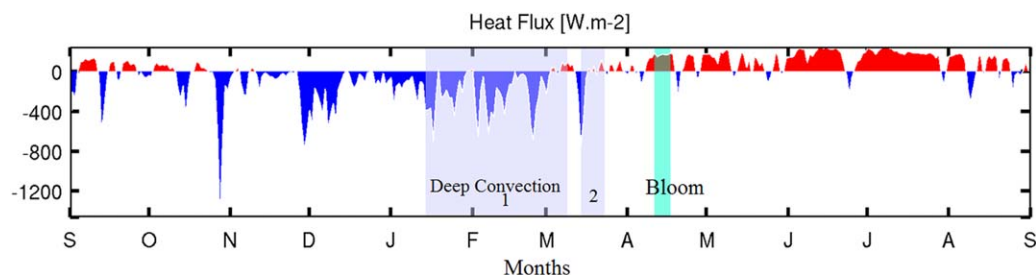


Figure 7. Time series of modeled total heat flux (W m^{-2}) at LION (indicated in Figure 1a) from September 2012 to September 2013. Blue bars represent the period when the MLD was higher than 1,000 m (convective mixing), while the green bar represents the restratification period coinciding with the phytoplankton development maximum.

convection event, from mid-January to early March, and a secondary convection event occurring during the third week of March. During the last week of March, the heat flux became durably positive in general. The frequency of the short, intense wind events decreased from three per month in April to one per month in summer. After March, the heat gain was a component of the progressive surface layer restratification, the development of instabilities around the mixed patch being the other component (Estournel et al., 2016b). In spring, large variations (40 m) of the MLD (Figure 8) can be noted because of the wind effect on a weak stratified surface layer, as during the third week of April.

4.1.2. Stock of Nutrients in the Upper Layer

Figure 9 presents the annual cycle of the simulated nitrate and phosphate stocks in the upper 130 m of the deep convection area. Stocks deduced from the cruise observations (see section 2.4 for details) are shown as horizontal bars overlaying the model output. The model reproduces the trend and orders of magnitude of the nutrient stock as estimated from the observations made during the three cruises, in winter ($800 \text{ mmol N m}^{-2}$ and 35 mmol P m^{-2}), spring ($<450 \text{ mmol N m}^{-2}$ and 20 mmol P m^{-2}), and summer ($<200 \text{ mmol N m}^{-2}$ and 10 mmol P m^{-2}). An underestimation of 10 mmol N m^{-2} (7% of the stock) for the stock of nitrate and 4 mmol P m^{-2} for the stock of phosphate (16% of the stock) is, however, visible in the model estimates for February 2013 when they are compared with the observations. In this section, we use the model outputs to analyze the impact of the physical and biogeochemical processes on the seasonal variations of the nutrient stock. The biogeochemical interfaces (nitracline, phosphacline and deep chlorophyll maximum [DCM]) are plotted in Figure 8. The year is divided into four periods corresponding to the seasons analyzed individually (they are indicated by colored vertical bars in Figures 8–11). The first season is autumn, from 1 September to 1 December 2012. Winter was chosen to start when both strong negative heat fluxes (from 1 December 2012 to 23 March 2013; Figure 7) and relatively deep mixed layer ($>50 \text{ m}$, Figure 8) conditions cooccurred. Spring, which begins on 24 March here, corresponds to the period where the mixed layer became shallower than the epipelagic layer, which was at 120 m in average (standard deviation: 30 m). It ends on 6 June when the mixed layer stabilized at very shallow depth ($<20 \text{ m}$) and the DCM

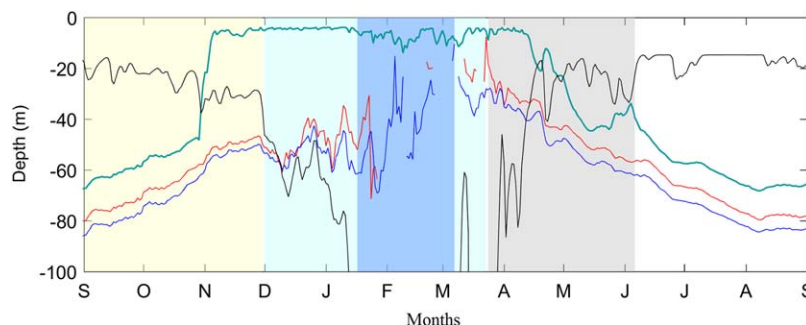


Figure 8. Time series of the depth (m) of the modeled mixed layer (in black), nitracline (in red), phosphacline (in blue), and deep chlorophyll maximum (in green) averaged over the deep convection region from September 2012 to September 2013. The background color stands for the season: yellow for autumn, blue for winter, with the dark blue representing the period when the MLD was higher than 1,000 m (convective mixing), gray for spring, and white for summer.

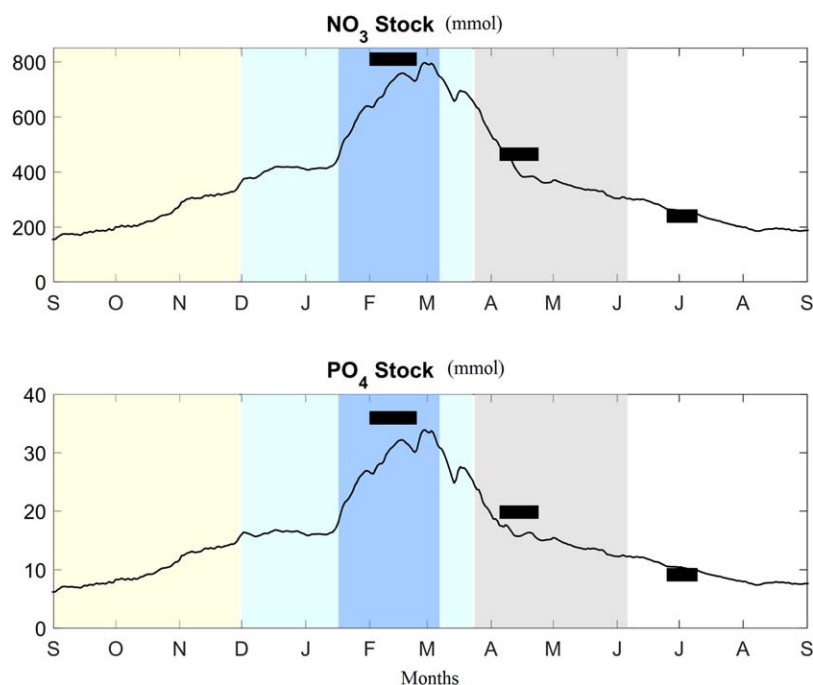


Figure 9. Time evolution of modeled (top) nitrate and (bottom) phosphate stocks (in mmol m^{-2}) in the upper layer (0–130 m) of the deep convection area from September 2012 to September 2013. Stock estimates derived from observations are shown as horizontal bars overlaying the model outputs. The four seasons identified in section 4.1.2 are indicated with background colors: yellow represents autumn, blue is for winter—with the dark blue representing the period when the MLD was higher than 1,000 m (deep convective mixing), gray is for spring, and white is for summer.

became established below 40 m. Summer is the last stage, which starts on 6 June and lasts until 1 September 2013, the end of the time series.

Figure 10 presents the annual cycle of the biogeochemical sink and source terms of nitrate and phosphate as well as the trends induced by vertical hydrodynamics, for the period 2012–2013. From early September to the end of October 2012, a shallowing of the nutricline from 80 to 60 m was modeled (standard deviation of 20 m). This upward displacement of the nutricline (Figure 8) could be induced by the isopycnal doming during the preconditioning phase of the deep convection process in the NW Med (Marshall & Schott, 1999) and/or by the variation of light intensity (Mignot et al., 2014). This led to a low but continuous increase of the nutrient stock in the upper layer (Figure 9). At the same time, the uptake of nutrients decreased continuously (Figure 10b). From October to November 2012, uptake of nitrate (respectively phosphate) became lower than nitrification (respectively excretion of phosphate). Therefore, the net effects of both physical and biogeochemical processes led to an increase of the nutrient stock in the upper layer (Figure 9).

The sudden northern wind event occurring at the end of November—beginning of December (Figure 7), thickening the ML to 50–60 m depth on average, close to the depth of the nutricline (Figure 8), led to an abrupt import of nutrients into the surface layer (Figure 10a), which were rapidly assimilated by phytoplankton (Figure 10b). This was followed by a progressive increase of phosphate excretion (Figure 10c), reflecting the triggering of the development of heterotrophs. Regarding the surface nutrients stock, after the wind gust of early December, the balance of source (vertical import and nitrification/phosphate excretion) and sink (mainly uptake) terms explains the nearly constant stocks (Figure 9).

The deep convection mixing, beginning in mid-January when the MLD exceeded 100 m (Figure 8), led to a large upwelling of inorganic nutrients to the surface layer (Figure 10a). The deep convection event also caused a sudden reduction of nitrate and phosphate uptake which, nevertheless, remained nonnegligible (Figure 10b). The phytoplankton biomass was vertically mixed, and preys and predators were then decoupled as shown by Auger et al. (2014). This resulted in an increase of the zooplankton mortality as shown by the intense drop of excretion rates during this period (Figure 10c). The decrease of ammonium and phosphate excretion rates was higher than the decrease of nitrate and phosphate uptake rates. It is

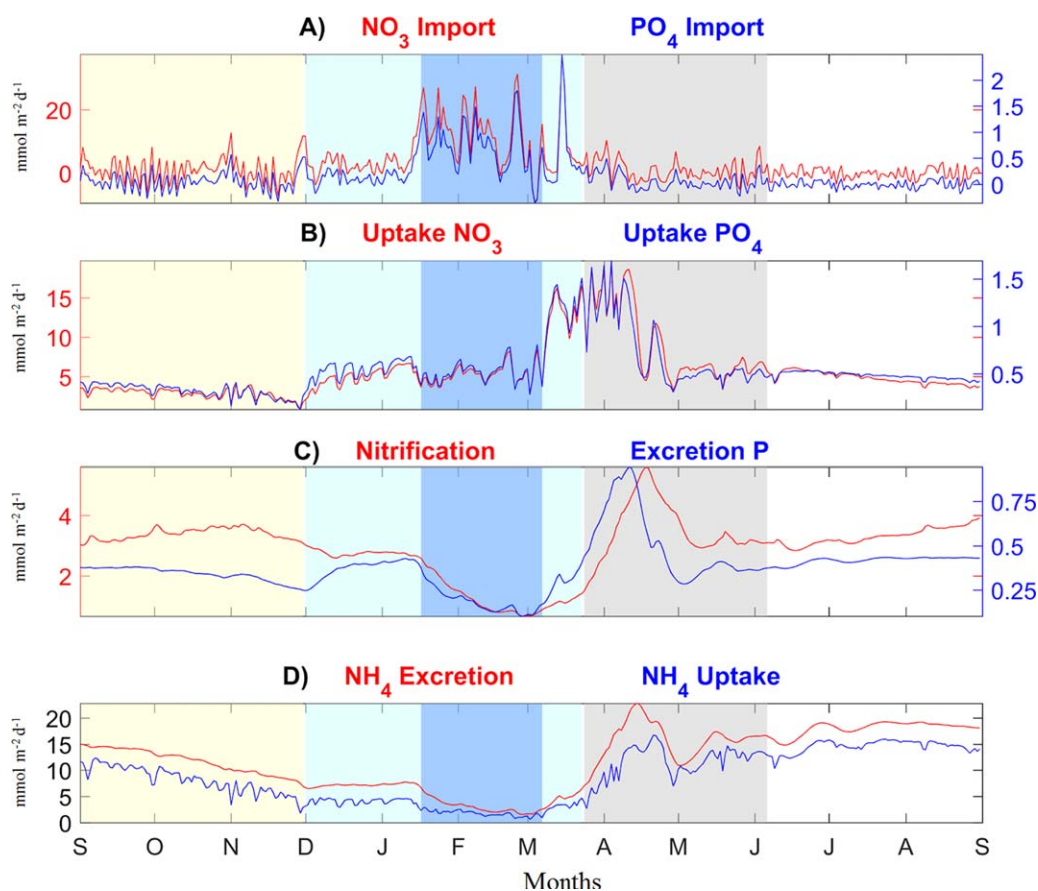


Figure 10. Time series of physical and biogeochemical fluxes that impact the stock of the inorganic nitrogen and phosphorus in the surface layer (0–130 m) from September 2012 to September 2013. These fluxes are inferred from the model and averaged over the open deep convection area. (a) Net import due to vertical advection and turbulent mixing of nitrate (red) and of phosphate (blue) into the surface layer, (b) uptake of nitrate (red) and phosphate (blue), (c) nitrification (red) and inorganic phosphorus excretion rates (blue), and (d) ammonia excretion (red) and uptake (blue). Units: $\text{mmol m}^{-2} \text{d}^{-1}$.

noteworthy that the uptake of nitrate (mean value: $6.4 \text{ mmol N m}^{-2} \text{d}^{-1}$) was higher than the uptake of ammonium (mean value: $1.9 \text{ mmol N m}^{-2} \text{d}^{-1}$) during deep convection (Figures 10b and 10d). Also, nitrification rate in the upper layer (mean value: $1.2 \text{ mmol N m}^{-2} \text{d}^{-1}$) was low during this intense mixing period (Figure 10c). Thus, during deep convection, nitrate and phosphate stock in the surface layer increased in the model (Figure 9) because of the nutrient convective supply and the reduced nutrient uptake. They reached their maximum in early March (Figure 9), when the main deep convection mixing stopped (Figure 8).

An intense phytoplankton development began during the second week of March, favored by the weakening of vertical mixing (not shown). This bloom was characterized by a sudden, strong consumption of nutrients (Figure 10b) that provoked a first sharp decrease of their surface stocks (Figure 9).

From the end of March to mid-April, nitrate and phosphate uptake remained strong (Figure 10b; phytoplankton biomass reached its maximum in mid-April, not shown). In parallel, excretion increased rapidly (Figures 10c and 10d). In mid-April, the reduction of vertical mixing (Figure 10a) led to a clear decrease of the vertical enrichment of the upper layer in nutrients. At this period, a strong decrease of nutrient uptake occurred. At the end of April, a new wind gust induced a brief deepening of the mixed layer (Figure 8) that enriched the surface layer in nutrients. A last strong, short pulse of nutrient uptake (Figure 10b) was then observed. Afterward, the nitrate and phosphate stock continuously decreased (Figure 9), and the nutricline and DCM depth increased (Figure 8). It is important to note that, after this last strong wind event, ammonium uptake dominated the total nitrogen uptake (Figures 10b and 10d). Regarding the nutrient stock, it

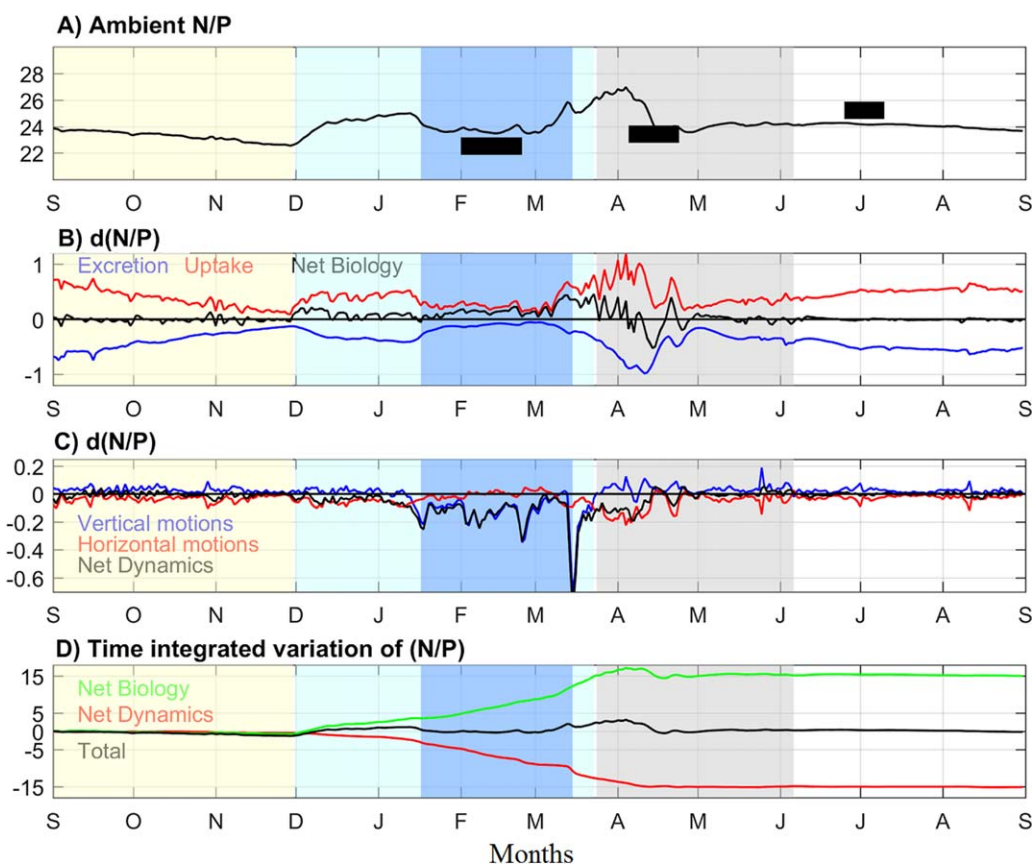


Figure 11. (a) Time series of the modeled N:P ratio (mol N mol P^{-1}) averaged in the upper layer (0–130 m) of the deep convection area from September 2012 to September 2013. Estimates from observations are shown as horizontal bars overlaying the model output. (b) Biogeochemical and (c) physical processes ($\text{mol N mol P}^{-1} \text{d}^{-1}$) influencing the N:P dynamics and (d) their net time integrated resultant.

can be concluded that, during the spring period, the strong rate of uptake (higher than the excretion and nitrification rate) explains the strong decreasing trend (Figure 9).

From June to August, the surface layer was depleted in nutrients (Figures 8 and 9). The model indicates an increase of the phosphate and ammonium excretion as well as of the nitrification rate (Figures 10c and 10d). The vertical physical flux was very weak (Figure 10a) and the net biogeochemical flux resulted in a low, continuous decrease of the nitrate and phosphate surface layer stock until the beginning of August, when it reached the value of November 2012 (Figure 8). In August, as the DCM and nutricline depths, the nutrient stock stabilized.

The trend of the contribution of nitrate and ammonium uptake in the total nitrogen uptake, shown in late spring, remained throughout the summer as the trophic regime was dominated by regenerated production, ammonium being continuously produced (Figure 10d), while nitrate was weakly imported from intermediate layers (Figure 10a). During summer, nitrification increased slightly but continuously (from 3 to 4 $\text{mmol m}^{-2} \text{d}^{-1}$, Figure 10c). It constituted from ~60 to 100% of nitrate uptake. The simulated nitrification rate presents the same order of magnitude as the measurements of Bianchi et al. (1999) who reported a rate of 1.4 $\text{mmol m}^{-2} \text{d}^{-1}$ within the DCM in the NW deep sea. In the model results, we found a value of 1.8 $\text{mmol m}^{-2} \text{d}^{-1}$ (25% higher than in the observations of Bianchi et al., 1999) by integrating nitrification only within the DCM in the deep convection area.

4.1.3. N:P Ratio in the Upper Layer

In marine ecology, the nitrate to phosphate ratio was determined to be universally 16:1 because of the phytoplankton requirements which control the marine biogeochemistry (Redfield et al., 1963). Even if this averaged ratio has been reappraised several times (Banse & English, 1994; Geider & La Roche, 2002), its

dynamics can still be used to understand the nitrogen and the phosphorus reactivity (Arrigo, 2005). Indeed, the N:P stoichiometry reflects relations between several processes: nutrients uptake by phytoplankton and small heterotrophs, rate of mineralization of organic matter, inorganic matter excretion by heterotrophs and finally the effects of physical processes (mixing and advection).

In the Mediterranean Sea, the ratio N:P is higher than the canonical value of 16:1. It was estimated on average at 24 (Pujo-Pay et al., 2011) with a pronounced horizontal gradient from west to east. To the west, the ratio is 22 in the Levantine Intermediate Water and the Western Mediterranean Deep Water while in the Levantine Basin, the ratio reaches 27 ± 3 :1 below 200 m (Ribera d'Alcalà et al., 2003). The N:P ratio can be much higher above the thermocline (Raimbault & Coste, 1990) because of the preference of phytoplankton for phosphate compared to nitrate. These ratios confirm that the Mediterranean waters are limited by phosphate, especially in the eastern basin.

In this section, we use our simulation to characterize the time evolution of the stoichiometry in the upper layer of the deep convection area, playing a key role in the water mass biogeochemical characteristics in the Mediterranean Sea, and to quantify the impact of the physical and biogeochemical processes responsible for their seasonal variations, over the period September 2012 to September 2013. The N:P ratio generally presents a negative gradient in the water column as observed in previous observational studies (Huertas et al., 2012; Pasqueron de Fommervault et al., 2015a; Pujo-Pay et al., 2011; Severin et al., 2014). The deep value (averaged between 130 m and the seafloor in the deep convection area, not shown) is 22.4 on average (standard deviation: 0.5) in the model results (it is 21.7 on average, standard deviation: 0.6 according to the interpolation of Dewex cruise observations). The maximum N:P vertical gradient is located below the nutricline (not shown). The N:P ratio presents higher variability in the surface layer than in deep layers (Pasqueron de Fommervault et al., 2015a, 2015b).

Figure 11a shows the time series of the spatially averaged N:P ratio in the upper layer of the deep convection area. N:P ratio deduced from the three cruise observations are also indicated by horizontal bars. Since the underestimation of phosphate stock is more pronounced than that of nitrate stock in the model during the winter cruise (Figure 9), the model overestimates the N:P ratio during this period. Besides, the overestimation of phosphate stock during MOOSE cruise period lead to an underestimation of N:P ratio during the summer period.

A first general remark about the effect of physical and biogeochemical processes on N:P is that uptake increases seawater N:P ratio while release of nitrate and phosphate decreases N:P (Figure 11b). The N:P ratio of uptake is lower than the ratio in seawater, which presents an excess of nitrate compared to phosphate. The effect of uptake is then to increase the water N:P ratio. For the same reason, the release of nutrients by the ecosystem produces a decrease of water N:P. A second remark is that convective mixing events characterized by depths >200 m produce a decrease of surface N:P ratio because of the general negative gradient of N:P.

At the beginning of September 2012, the spatial mean N:P ratio was 24.1 (standard deviation: 0.5) according to the model (Figure 11a). From September to December 2012, the influence of each physical process on the N:P ratio was lower than the effect of the biogeochemical processes (Figures 11c and 11d). Yet both physical and biogeochemical processes had a negative impact on N:P (-0.7 for the net effect of the biogeochemical processes and -0.5 for the net effect of physical processes), explaining its slow and regular decrease.

From December 2012 to mid-January 2013, when nitrate and phosphate uptake rates were higher than the nitrification and phosphate excretion, respectively, the biogeochemical processes tended to strongly increase the N:P ratio (Figures 11b and 11d). In parallel, the horizontal dynamics tended to slightly decrease the N:P ratio. The resulting evolution was a rapid increase of the N:P ratio from 22.8 to 24.2 in the first 15 days of the autumnal bloom (1 December to 15 December), and a second slow increase from 24.2 to 25 during the following month (15 December to 15 January).

During the main convective period (16 January to 7 March 2013), the contributions of individual biogeochemical processes to N:P variations were low (Figure 11b). Besides, the strong deepening of the mixed layer in mid-January induced a rapid decrease of surface N:P, due to vertical imports of lower N:P deep waters (Figure 11c). During the rest of the convective period, the N:P ratio reached a relatively stationary

phase: the positive trend of the nutrient uptake that dominated the biology was balanced by the negative trend of the vertical mixing. During this period, the model N:P ratio was around 23, which is close to the mean value of 22.5 (standard deviation: 0.6) deduced from the observations of the February cruise. This difference between the two ratios could be explained by an underestimation of the N:P ratio of the deep waters at the model initialization.

Then, the sudden and strong consumption of nutrients at the onset of the winter/spring bloom induced a pronounced increase of the N:P ratio to 26 (Figures 11a and 11b). This increase was interrupted during the secondary convective mixing of the third week of March, inducing a small decrease of the N:P ratio of 0.3 (Figure 11c).

The period with the highest N:P ratio corresponds to the transition between winter and spring (late March to early April) when the phytoplankton growth and nutrient uptake were strong (Figures 10b and 11a). In early April, phosphate excretion increased proportionally more rapidly than the production of nitrate by nitrification (Figure 10c). This induced a decrease of the N:P ratio (Figures 11b and 11d), intensified by the effect of vertical physical processes.

From mid-April, the contribution of physical processes to the variations of N:P was very low, N:P being mostly affected by the balance between excretion and uptake processes. The time lag between excretion of phosphate, nitrification and uptakes of nitrate and phosphate, as well as the difference in the rate of these processes, produced a biogeochemical contribution that was alternately positive and negative, with a decreasing trend until the end of spring.

From early June to early August, the effect of vertical motions balanced the effect of horizontal motions, and, likewise, the effect of uptake processes balanced the effect of production processes. Overall, the variations of N:P were negligible. For the period of the MOOSE summer cruise, the modeled N:P (24.2) is close to the ratio deduced from observations (25.1).

Our results shows that the N:P ratio was submitted to strong changes in the upper layer at the beginning of phytoplankton blooms. Those rapid modeled increases of N:P ratio, reflecting a phosphorus limitation for phytoplankton growth, are in agreement with the increase measured by Severin et al. (2014) in March 2011 after restratification. This is also coherent with the results of Lazzari et al. (2016), based on 3-D modeling on the whole Mediterranean sea, indicating a limitation of primary production by phosphate in our study area. Two other rapid changes (decrease) were also modeled during the studied period. The first modeled decrease of N:P ratio in the upper layer occurring at the beginning of the deep convection event is coherent with the negative vertical gradient observed in the study region. The second modeled decrease occurred when uptake of nitrate by phytoplankton started to decrease after the peak of the spring bloom. This should be addressed and confirmed with further observations.

4.2. Annual Budgets of Nitrogen and Phosphorus

The annual nitrogen and phosphorus budgets of the deep convection area were calculated with the model in the upper layer (0–130 m) and in the deep layer (130 m to seafloor; Figure 12). The total stocks of nitrogen and phosphorus in this area exhibit a variation of -0.37% for nitrogen and -1.37% for phosphorus between September 2012 and September 2013.

The annual net vertical import of nitrate and phosphate is estimated at $1,029 \text{ mmol N m}^{-2} \text{ yr}^{-1}$ and $59 \text{ mmol P m}^{-2} \text{ yr}^{-1}$, respectively. The nutrient vertical supply occurring over the convection period (17 January to 17 March) corresponds to 68% of the annual vertical supply. According to the comparison exercise (section 3), it may have been underestimated. The simulated vertical nutrients import is of the same order of magnitude as previous estimates for the NW Med (Pujo-Pay & Conan, 2003; Severin et al., 2014; Table 1). It is also of the same order of magnitude as the estimation of $1400 \text{ mmol N m}^{-2} \text{ yr}^{-1}$ in the convective Atlantic subpolar region (Williams & McLaren, 2000). The annual lateral exports of nitrate and phosphate from the surface layer of the convection zone, to the surrounding areas, are low and are estimated at $5 \text{ mmol N m}^{-2} \text{ yr}^{-1}$ and $2 \text{ mmol P m}^{-2} \text{ yr}^{-1}$, respectively.

Regarding the biogeochemical processes budget in the surface layer, the consumption of nitrate and ammonium makes up 39% and 61%, respectively, of the total nitrogen uptake. The annual production of nitrate by nitrification is 103% of the annual nitrate supply from deep waters and 50% of the nitrate uptake. Therefore, the new production as defined by Dugdale and Goering (1967; primary production fueled by

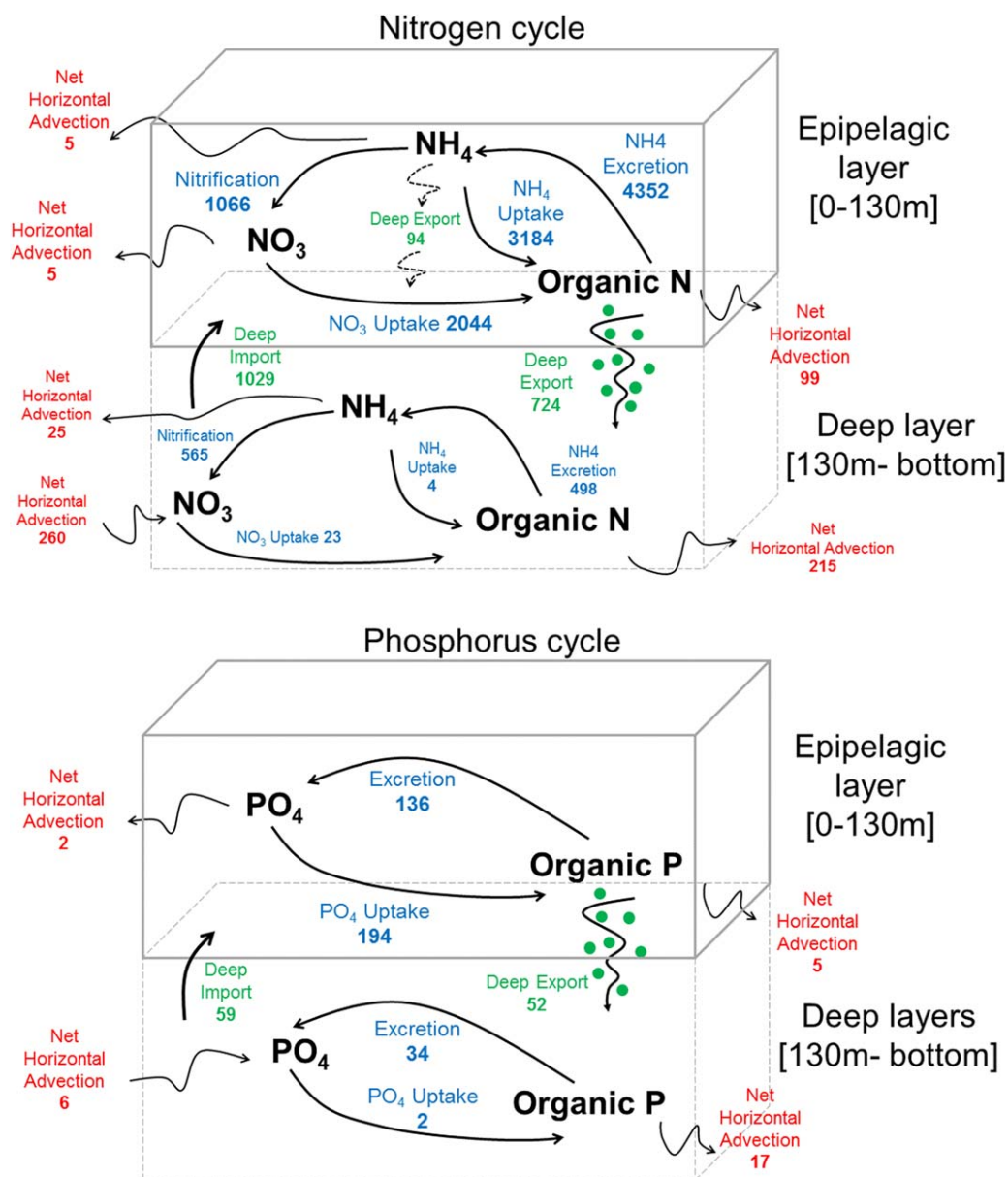


Figure 12. Modeled annual fluxes of (top) nitrogen and (bottom) phosphorus in the deep convection region (in $\text{mmol m}^{-2} \text{yr}^{-1}$) over the period from September 2012 to September 2013.

nonregenerated nutrients) could be overestimated by 100% if nitrification rates are taken into account in the calculation. Our results are coherent with those of Raimbault et al. (1998), who showed a 20%–100% overestimation of new primary production in the Pacific Ocean when nitrification was not taken into account in the calculation. They agree also with those of Dore and Karl (1996), who established that 47–142% of the nitrate assimilated by primary producers was produced by nitrification at the ALOHA oligotrophic station, and those of Martin and Pondaven (2006) who found that uptake of regenerated nitrate through nitrification constituted 22–57% of the total nitrate uptake. Our results are also close to the results of Gentilhomme (1992) who found that nitrification represented 23% of total nitrogen uptake (18% in this study) in the Algerian basin. From a quantitative point of view, using the Redfield ratio to facilitate comparison with previous studies, we have obtained a new production ranging between 77 and 162 $\text{g C m}^{-2} \text{yr}^{-1}$, depending on whether nitrification is considered in the calculation. As mentioned in section 2.3, the choice of a constant depth corresponding to the base of the productive layer could lead to an overestimation of the new production. Indeed, as demonstrated by previous studies (Körtzinger et al., 2008; Martin &

Table 1
Compilation of Nutrient Flux Estimates in the Northwestern Mediterranean Open Sea

Process	Unit	Reference	Period	Values	
Vertical import of inorganic nutrients	mmol m ⁻² yr ⁻¹			NO3 P04	
		Pujo-Pay and Conan (2003)	1993	433–650	
		Severin et al. (2014)	Feb/Mar 2011 convection events	760/800	36/36
		This study	2013 deep convection event	674	40
New production	mg C m ⁻² yr ⁻¹	This study	Sep 2012 to Sep 2013	1,029	59
		Severin et al. (2014)	Feb/Mar 2011		46/63
		This study	Sep 2012 to Sep 2013	65–77	
Export of organic matter	mmol m ⁻² yr ⁻¹				
		Pujo-Pay and Conan (2003)	1993	274–814	
		This study	Sep 2012 to Sep 2013		724

Pondaven, 2006; Palevsky et al., 2016), nitrate originating from the recycling of organic matter exported downward during deep mixing periods could have been reinjected in the upper layer. We estimate nitrification in the deep layer during deep convection period at 158 mmol m⁻² (28% of the annual deep nitrification). If the whole nitrate produced by nitrification in the deep layer during convection period is reinjected in the upper layer and used by phytoplankton for its growth, then our estimate of new production is overestimated by 13 g C m⁻² yr⁻¹ (using a Redfield ratio). The lower values of our estimate of new production (65–77 g C m⁻² yr⁻¹) are in the range of a previous estimate for the offshore NW Med (Table 1), a region that exhibits the highest values in the open Mediterranean Sea (Béthoux, 1989).

The net amount of organic matter produced in the surface layer is mostly exported toward the deep layer. The amount of produced organic matter advected horizontally toward the adjacent surface regions represents a small percentage of the net amount produced: 11% of the total organic nitrogen and 9% of the total organic phosphorus. The vertical export to the deep layer of dissolved and particulate organic nitrogen and phosphorus is estimated at 724 mmol N m⁻² yr⁻¹ and 52 mmol P m⁻² yr⁻¹, respectively. These estimates are in the same order of magnitude as the estimates in Pujo-Pay and Conan (2003; Table 1). During the convection period (17 January to 17 March), the export represents 55% of the annual amount of organic nitrogen and 58% of the annual amount of organic phosphorus. Two thirds of the total exported organic matter is remineralized by heterotrophs and one third is advected to the surrounding deep regions. With respect to the deepwater biogeochemical nitrogen cycle, the ammonium produced by remineralization is mostly transformed into nitrate by nitrification. The difference in the nitrification:uptake of ammonium ratio (<1 in the upper layer and >1 in the deep layer) in upper and deep layer is explained by both higher ammonium uptake rates in the upper layer and lower nitrification rates due to an inhibition effect by light in the upper layer. An annual import of nitrate (260 mmol N m⁻² yr⁻¹) and phosphate (6 mmol P m⁻² yr⁻¹) is obtained by horizontal advection in the deep layer. It is worth noting that this net horizontal supply results from two strong opposite fluxes: an import of 936 mmol N m⁻² yr⁻¹ for nitrate and of 39 mmol P m⁻² yr⁻¹ for phosphate in the intermediate waters (between 130 and 800 m) and an export of 676 mmol N m⁻² yr⁻¹ for nitrate and of 33 mmol P m⁻² yr⁻¹ for phosphate in the deep waters (below 800 m).

The model results suggest that, at the annual scale, the deep convection area appears as an autotrophic system (uptake rates dominate excretion rates) where deep inorganic nutrients injected in the surface layer are almost entirely consumed by phytoplankton. Our estimates for the period 2012–2013 suggest that, at the scale of the Mediterranean Sea, the total vertical supply by physical processes in the NW deep convection region could constitute a major source of nutrients in the surface layer compared to the terrestrial and atmospheric inputs (Krom et al., 2004; Ribera d'Alcalà et al., 2003; Table 2).

Atmospheric deposition and nitrogen fixation were not taken into account in the simulation. Results of previous studies suggested that they would have little influence on the annual N and P budget in the NW Med deep convection region, where there is a large vertical supply of nutrients. Aphotic nitrogen fixation was

Table 2*Estimates of the Net Inputs of Nitrogen and Phosphorus in the Surface Layer in the Mediterranean Sea (in 10^6 mol yr^{-1})*

Sources in the surface layer	N	P	Reference
Atmospheric inputs in the western basin	10,042–72,825	357–697	Ribera d'Alcalà et al. (2003)
Terrestrial inputs in the western basin	7,840–18,020	168–1,258	Ribera d'Alcalà et al. (2003)
Atmospheric inputs in the eastern basin	6,064–73,621	379–957	Ribera d'Alcalà et al. (2003)
	111,000	950	Krom et al. (2004)
Terrestrial inputs in the eastern basin	11,592–77,519	248–1,541	Ribera d'Alcalà et al. (2003)
	63,000	2,400	Krom et al. (2004)
Vertical physical inputs in the NW Med deep convection area	63,474	3,640	This study

shown to contribute 0.5% of the total nitrogen inputs in the whole Mediterranean basin (Benavides et al., 2016). Regarding the atmospheric deposition, Lazzari et al. (2012), using coupled modeling, showed that atmospheric and terrestrial inputs led to a 5% increase in the net primary production. The experiments performed by Ridame and Guieu (2002) showed that, in the western Mediterranean, the inputs of Saharan dissolved inorganic phosphorus had a negligible impact on the new production integrated over the productive layer, at the scale of the oligotrophic period, when the contribution of atmospheric deposition to the total nutrient input to the euphotic layer is largest.

The budget of the present study was obtained using a given coupled model and for a 1 year period. Multi-year simulations would allow the variability of these terms in response to the interannual variability of atmospheric and ocean conditions to be evaluated. Moreover, uncertainties on the various terms of this budget could be estimated from additional experiments based on other coupled models.

5. Conclusion and Perspectives

A coupled physical-biogeochemical model was compared to a high-resolution data set of three seasons of the same year (2013) and Bio-Argo float data, which document a strong convective winter, a phytoplankton bloom and an oligotrophic period in the NW Med. Despite some limits highlighted through the comparisons with observations, the model was shown to be able to reproduce the general observed seasonal dynamics of the physical and biogeochemical events correctly.

Our study shows that injections of nutrients during the wind intensification period triggered the autumn bloom. Then, convection in winter upwelled large amounts of nutrients into the upper layer. Decoupling of phytoplankton and zooplankton due to dilution as suggested by the collapse of heterotrophs when the mixed layer deepened strongly (mid-January), reduced the grazing pressure. When the conditions for phytoplankton development were all present (reduction of vertical mixing, low grazing pressure), a bloom was triggered with a massive consumption of nutrients during more than 1 month, resulting in a depletion of nutrients at the surface by the end of April. Nutrient consumption continued to deplete nutrients at increasing depths, inducing a deepening of the nutricline and DCM. This finally led to the summer oligotrophy of the water column.

The N:P ratio changed mainly through physical or biogeochemical processes during transition periods. First, during the intense convection mixing, the large enrichment of surface waters in deep nutrients suddenly reduced the surface N:P ratio. Second, during the beginning of the bloom, the predominance of high nutrient uptake over low excretion induced a strong increase of the N:P. Thirdly, during the peak of the bloom when the nutrient stock decreased strongly, uptake decreased, and excretion was maximum. Nitrification created a decoupling in the recycling of nutrients, decreasing the ratio N:P. At the annual scale, the surface N:P ratio did not appear to be impacted by the intense vertical mixing and spring bloom induced by the deep convection.

At the annual scale and for the studied year, the dense water formation area was a sink of nitrate and phosphate in intermediate layers, and a source of organic nitrogen and phosphorus throughout the water column, for the surrounding regions (Figure 13). The upward nutrient fluxes into the surficial NW Med deep

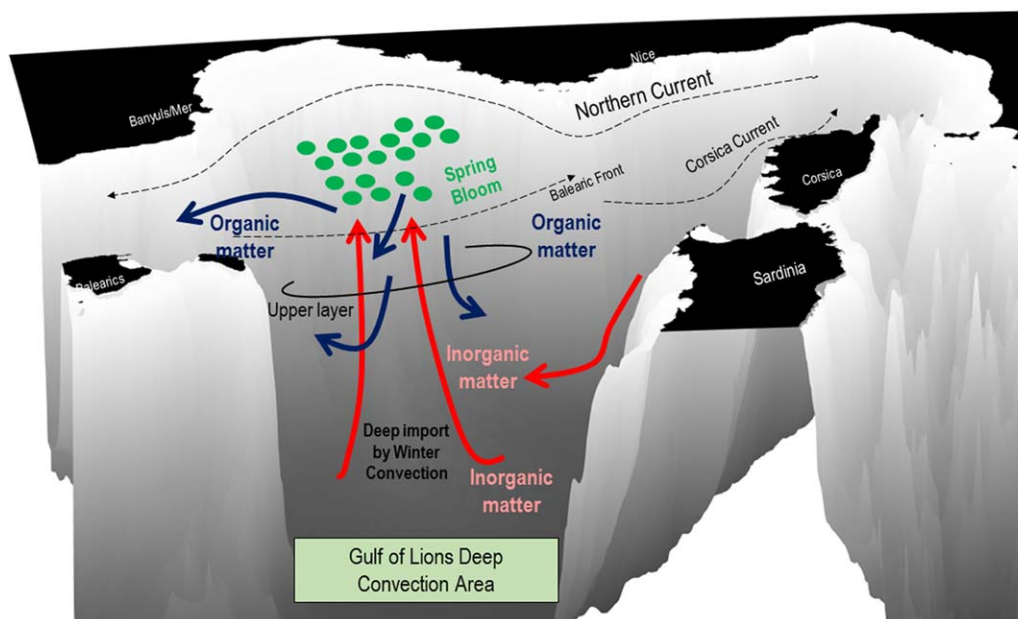


Figure 13. Conceptual model of the main processes driving the organic and inorganic matter dynamics in the NW Mediterranean Sea over the period from September 2012 to September 2013.

convection area is estimated to be in the same order of magnitude as the atmospheric and terrestrial inputs of each of the western and eastern subbasins of the Mediterranean Sea.

Further multiyear simulations from the coupled model will be used to better understand and quantify the impact of atmospheric and ocean interannual variability of the pelagic ecosystem and associated carbon, nitrogen and phosphorus cycles in this region. Previous studies suggested that deep convection could be strongly weakened (Somot et al., 2006; Adloff et al., 2015) or strengthened (Adloff et al., 2015) by the end of XXI century. We will then use the coupled model to explore and quantify how climate change and anthropogenic forcing may alter the NW Med deep convection biogeochemical cycles, in particular the nutrient vertical supply in the euphotic layer and the new production, in the near future.

Acknowledgments

This study has been funded by the PERSEUS project (European Union FP7 grant 287600). It is a contribution to the MerMex (Marine Ecosystem Response in the Mediterranean Experiment. <https://doi.org/10.17600/13020010>, <https://doi.org/10.17600/13020030>, and <https://doi.org/10.17600/13450110>), particularly DeWEX and MOOSE projects project of the MISTRALS international program. Numerical simulations were performed using the computing cluster of Laboratoire d'Aérodynamique et HPC resources from CALMIP (grants P1325 and P1331). The biogeochemical floats have been funded by the French NAOS project (Investissement d'Avenir, ANR J11R107-F). These data were collected and made freely available by the International Argo Program and the national programs that contribute to it. (<http://www.argo.ucsd.edu>, <http://argo.jcommops.org>). The Argo Program is part of the Global Ocean Observing System. (<http://doi.org/10.17882/42182>).

References

- Adloff, F., Somot, S., Sevault, F., Jordà, G., Aznar, R., Déqué, M., . . . Gomis, D. (2015). Mediterranean Sea response to climate change in an ensemble of twenty first century scenarios. *Climate Dynamics*, 45, 2775–2802. <https://doi.org/10.1007/s00382-015-2507-3>
- Allen, J. I., Somerfield, P., & Gilbert, F. (2007). Quantifying uncertainty in high-resolution coupled hydrodynamic-ecosystem models. *Journal of Marine Systems*, 64, 3–14. <https://doi.org/10.1016/j.jmarsys.2006.02.010>
- Anderson, T. R., & Pondaven, P. (2003). Non-redfield carbon and nitrogen cycling in the Sargasso Sea: Pelagic imbalances and export flux. *Deep Sea Research Part I: Oceanographic Research Papers*, 50, 573–591.
- Antoine, D., Morel, A., Gordon, H. R., Banzon, V. F., & Evans, R. H. (2005). Bridging ocean color observations of the 1980s and 2000s in search of long-term trends. *Journal of Geophysical Research*, 110, C06009. <https://doi.org/10.1029/2004JC002620>
- Arrigo, K. R. (2005). Marine microorganisms and global nutrient cycles. *Nature*, 437, 349–355. <https://doi.org/10.1038/nature04159>
- Auger, P., Diaz, F., Ulses, C., Estournel, C., Neveux, J., Joux, F., . . . Naudin, J.-J. (2011). Functioning of the planktonic ecosystem on the Gulf of Lions shelf (NW Mediterranean) during spring and its impact on the carbon deposition: A field data and 3-D modelling combined approach. *Biogeochemistry*, 8(11), 3231–3261. <https://doi.org/10.5194/bg-8-3231-2011>
- Auger, P., Ulses, C., Estournel, C., Stemann, L., Somot, S., & Diaz, F. (2014). Interannual control of plankton communities by deep winter mixing and prey/predator interactions in the NW Mediterranean: Results from a 30-year 3D modeling study. *Progress in Oceanography*, 71, 12–27. <https://doi.org/10.1016/j.pocean.2014.04.004>
- Baklouti, M., Faure, V., Pawlowski, L., & Sciandra, A. (2006). Investigation and sensitivity analysis of a mechanistic phytoplankton model implemented in a new modular numerical tool (Eco3M) dedicated to biogeochemical modelling. *Progress in Oceanography*, 71(1), 34–58. <https://doi.org/10.1016/j.pocean.2006.05.003>
- Banase, K., & English, D. C. (1994). Seasonality of coastal zone color scanner phytoplankton pigment in the offshore oceans. *Journal of Geophysical Research*, 99(C4), 7323–7345. <https://doi.org/10.1029/93JC02155>
- Behrenfeld, M. J. (2010). Abandoning Sverdrup's critical depth hypothesis on phytoplankton blooms. *Ecology*, 91, 977–989.
- Benavides, M., Bonnet, S., Hernández, N., Martínez-Pérez, A. M., Nieto-Cid, M., Álvarez-Salgado, X. A., . . . Aristegui, J. (2016). Basin-wide N_2 fixation in the deep waters of the Mediterranean Sea. *Global Biogeochemical Cycles*, 30, 952–961. <https://doi.org/10.1002/2015GB005326>
- Bentsen, M., Evensen, G., Drange, H., & Jenkins, A. D. (1999). Coordinate transformation on a sphere using conformal mapping. *Monthly Weather Review*, 127, 2733–2740.

- Béthoux, J. P. (1989). Oxygen consumption, new production, vertical advection and environmental evolution in the Mediterranean Sea. *Deep Sea Research Part A. Oceanographic Research Papers*, 36(5), 769–781. [https://doi.org/10.1016/0198-0149\(89\)90150-7](https://doi.org/10.1016/0198-0149(89)90150-7)
- Béthoux, J. P., Morin, P., Chaumery, C., Connan, O., Gentili, B., & Ruiz-Pino, D. (1998). Nutrients in the Mediterranean Sea, mass balance and statistical analysis of concentrations with respect to environmental change. *Marine Chemistry*, 63(1–2), 155–169.
- Bianchi, M., Fosset, C., & Connan, P. (1999). Nitrification rates in the NW Mediterranean Sea. *Aquatic Microbial Ecology*, 17, 267–278.
- Butenschön, M., Zavatarelli, M., & Vichi, M. (2012). Sensitivity of a marine coupled physical biogeochemical model to time resolution, integration scheme and time splitting method. *Ocean Modelling*, 52–53, 36–53. <https://doi.org/10.1016/j.ocemod.2012.04.008>
- Conan, P. (2013). *DEWEX-MERMEX 2013 LEG2 cruise, RV Le Suroit*. Brest, France: SISMER. <https://doi.org/10.17600/13020030>
- Dilek, E., Yilmaz, A., & Tugrul, S. (2005). Vertical profiles of particulate organic matter and its relationship with chlorophyll-*a* in the upper layer of the NE Mediterranean Sea. *Journal of Marine Systems*, 55(3–4), 311–326.
- Dore, J. E., & Karl, D. M. (1996). Nitrification in the euphotic zone as a source for nitrite, nitrate, and nitrous oxide at Station ALOHA. *Limnology and Oceanography*, 41, 1619–1628.
- D'Ortenzio, F., Lavigne, H., Besson, F., Claustre, H., Coppola, L., Garcia, N., . . . Testor, P. (2014). Observing mixed layer depth, nitrate and chlorophyll concentrations in the northwestern Mediterranean: A combined satellite and NO₃ profiling floats experiment. *Geophysical Research Letters*, 41, 6443–6451. <https://doi.org/10.1002/2014GL01020>
- D'Ortenzio, F., & Ribera d'Alcalá, M. (2009). On the trophic regimes of the Mediterranean Sea: A satellite analysis. *Biogeosciences*, 6, 139–148.
- Dugdale, R. C., & Goering, J. J. (1967). Uptake of new and regenerated forms of nitrogen in primary productivity. *Limnology and Oceanography*, 12, 196–206.
- Durrieu de Madron, X., & Mermex Group. (2011). Marine ecosystems' responses to climatic and anthropogenic forcings in the Mediterranean. *Progress in Oceanography*, 91(2), 97–166. <https://doi.org/10.1016/j.poccean.2011.02.003>
- Estournel, C., Testor, P., Damien, P., D'Ortenzio, F., Marsaleix, P., Conan, P., . . . Prieur, L. (2016b). High resolution modeling of dense water formation in the north-western Mediterranean during winter 2012–2013: Processes and budget. *Journal of Geophysical Research: Oceans*, 121, 5367–5392. <https://doi.org/10.1002/2016JC011935>
- Estournel, C., Testor, P., Taupier-Letage, I., Bouin, M. N., Coppola, L., Durand, P., . . . Somot, S. (2016a). HyMeX-SOP2, the field campaign dedicated to dense water formation in the north-western Mediterranean. *Oceanography*, 29, 4.
- Estournel, C., Zervakis, V., Marsaleix, P., Papadopoulos, A., Auclair, F., Perivoliotis, L., & Tragou, E. (2005). Dense water formation and cascading in the Gulf of Thermaikos (North Aegean) from observations and modelling. *Continental Shelf Research*, 25, 2366–2386. <https://doi.org/10.1016/j.csr.2005.08.014>
- Estrada, M., Latasa, M., Emelianov, M., Gutiérrez-Rodríguez, A., Fernández-Castro, B., Isern-Fontanet, J., . . . Vidal, M. (2014). Seasonal and mesoscale variability of primary production in the deep winter-mixing region of the NW Mediterranean. *Deep Sea Research Part I: Oceanographic Research Papers*, 94, 45–61. <https://doi.org/10.1016/j.dsr.2014.08.003>
- Gaćić, M., Civitarese, G., Miserocchi, S., Cardin, V., Crise, A., & Mauri, E. (2002). The open-ocean convection in the Southern Adriatic: A controlling mechanism of the spring phytoplankton bloom. *Continental Shelf Research*, 22, 1897–1908. [https://doi.org/10.1016/S0278-4343\(02\)00050-X](https://doi.org/10.1016/S0278-4343(02)00050-X)
- Geider, R., & La Roche, J. (2002). Redfield revisited: Variability of C:N:P in marine microalgae and its biochemical basis. *European Journal of Phycology*, 37(1), 1–17. <https://doi.org/10.1017/S0967026201003456>
- Gentilhomme, V. (1992). *Quantification des flux d'absorption et de régénération de l'azote minéral (nitrate, nitrite, ammonium) et organique (urée) dans la couche euphotique des océans oligotrophes* (Thèse). Provence, France: Université Aix-Marseille.
- Gogou, A., Sanchez-Vidal, A., Durrieu de Madron, X., Stavrakakis, S., Calafat, A. M., Stabholz, M., . . . Papathanassiou, E. (2014). Reprint of: Carbon flux to the deep in three open sites of the Southern European Seas (SES). *Journal of Marine Systems*, 135, 170–179. <https://doi.org/10.1016/j.jmarsys.2014.04.012>
- Hauser, D., Branger, H., Bouffies-Cloché, S., Despiou, S., Drennan, W., Dupuis, H., . . . Weill, A. (2003). The FETCH experiment: An overview. *Journal of Geophysical Research*, 108(C3), 8053. <https://doi.org/10.1029/2001JC001202>
- Herrmann, M., Auger, P.-A., Ulse, C., & Estournel, C. (2017). Long-term monitoring of ocean deep convection using multisensors altimetry and ocean color satellite data. *Journal of Geophysical Research Oceans*, 122, 1457–1475. <https://doi.org/10.1002/2016JC011833>
- Herrmann, M., Diaz, F., Estournel, C., Marsaleix, P., & Ulse, C. (2013). Impact of atmospheric and oceanic interannual variability on the Northwestern Mediterranean Sea pelagic planktonic ecosystem and associated carbon cycle. *Journal of Geophysical Research: Oceans*, 118, 5792–5813. <https://doi.org/10.1002/jgrc.20405>
- Herrmann, M., Sevault, F., Beuvier, J., & Somot, S. (2010). What induced the exceptional 2005 convection event in the northwestern Mediterranean basin? Answers from a modeling study. *Journal Geophysical Research*, 115, C12051. <https://doi.org/10.1029/2010JC006162>
- Herrmann, M., Somot, S., Sevault, F., Estournel, C., & Déqué, M. (2008). Modeling the deep convection in the Northwestern Mediterranean sea using an eddy-permitting and an eddy-resolving model: Case study of winter 1986–87. *Journal of Geophysical Research*, 113, C04011. <https://doi.org/10.1029/2006JC003991>
- Houpert, L., Durrieu de Madron, X., Testor, P., Bosse, A., D'Ortenzio, F., Bouin M. N., . . . Raimbault, P. (2016). Observations of open-ocean deep convection in the northwestern Mediterranean Sea: Seasonal and interannual variability of mixing and deep water masses for the 2007–2013 Period. *Journal of Geophysical Research Oceans*, 121, 8139–8171. <http://dx.doi.org/10.1002/2016JC011857>
- Houpert, L., Testor, P., Durrieu de Madron, X., Somot, S., D'Ortenzio, F., Estournel, C., & Lavigne, H. (2015). Seasonal cycle of the mixed layer, the seasonal thermocline and the upper-ocean heat storage rate in the Mediterranean Sea derived from observations. *Progress in Oceanography*, 132 (2015), 333–352.
- Huertas, E., Rios, A. F., García-Lafuente, J., Navarro, G., Makaoui, A., Sánchez-Román, A., . . . Pérez, F. F. (2012). Atlantic forcing of the Mediterranean oligotrophy. *Global Biogeochemical Cycles*, 26, GB2022. <https://doi.org/10.1029/2011GB004167>
- Körtzinger, A., Send, U., Wallace, D. W. R., Kartensen, J., & DeGrandpre, M. (2008). Seasonal cycle of O₂ and pCO₂ in the central Labrador Sea: Atmospheric, biological, and physical implications. *Global Biogeochemical Cycles*, 22, GB1014. <https://doi.org/10.1029/2007GB003029>
- Krom, M. D., Herut, B., & Mantoura, R. F. C. (2004). Nutrient budget for the Eastern Mediterranean: Implications for phosphorus limitation. *Limnology and Oceanography*, 49, 1582–1592. <https://doi.org/10.4319/lo.2004.49.5.1582>
- Krom, M. D., Kress, N., Brenner, S., & Gordon, L. I. (1991). Phosphorus limitation of primary productivity in the eastern Mediterranean Sea. *Limnology and Oceanography*, 36, 424–432.
- Large, W. G., & Yeager, S. G. (2004). *Diurnal to decadal global forcing for ocean and sea-ice models: The data sets and flux climatologies* (NCAR Tech. Note NCAR/TN-460+STR). Boulder, CO: National Center of Atmospheric Research. <https://doi.org/10.5065/D6KK98Q6>
- Lavigne, H. (2013). *Impact of mixed layer depth seasonal variations on the phytoplankton phenology in the Mediterranean Sea* (PhD thesis). Paris, France: University Pierre et Marie Curie.

- Lavigne, H., D'Ortenzio, F., Ribera d'Alcalà, M., Claustre, H., Sauzède, R., & Gačić, M. (2015). On the vertical distribution of the chlorophyll *a* concentration in the Mediterranean Sea: A basin scale and seasonal approach. *Biogeoscience*, *12*, 5021–5039. <https://doi.org/10.5194/bg-12-5021-2015>
- Lazzari, P., Solidoro, C., Ibello, V., Salon, S., Teruzzi, A., Beranger, K., . . . Crise A. (2012). Seasonal and inter-annual variability of plankton chlorophyll and primary production in the Mediterranean Sea: A modeling approach. *Biogeosciences*, *9*, 217–233.
- Lazzari, P., Solidoro, C., Salon, S., & Bolzon, G. (2016). Spatial variability of phosphate and nitrate in the Mediterranean Sea: A modeling approach. *Deep Sea Research Part I: Oceanographic Research Papers*, *108*, 39–52. <https://doi.org/10.1016/j.dsr.2015.12.006>
- Lellouche, J.-M., Le Galloudec, O., Drévillon, M., Régnier, C., Greiner, E., Garric, G., . . . De Nicola, C. (2013). Evaluation of global monitoring and forecasting systems at Mercator Océan. *Ocean Science*, *9*, 57–81. <https://doi.org/10.5194/os-9-57-2013>
- Ludwig, W., Bouwman, A. F., Dumont, E., & Lespinas, F. (2010). Water and nutrient fluxes from major Mediterranean and Black Sea rivers: Past and future trends and their implications for the basin-scale budgets. *Global Biogeochemical Cycles*, *24*, GB0A13. <https://doi.org/10.1029/2009GB003594>
- Manca, M., Burca, M., Giorgetti, A., Coatanoan, C., Garcia, M. J., & Iona, A. (2004). Physical and biochemical averaged vertical profiles in the Mediterranean regions: An important tool to trace the climatology of water masses and to validate incoming data from operational oceanography. *Journal of Marine Systems*, *48*(1–4), 83–116.
- Maraldi, C., Chanut, J., Levier, B., Ayoub, N., De Mey, P., Reffray, G., . . . the Mercator Research and Development Team. (2013). NEMO on the shelf: Assessment of the Iberia–Biscay–Ireland configuration. *Ocean Science*, *9*, 745–771. <https://doi.org/10.5194/os-9-745-2013>
- Marsaleix, P., Auclair, F., Duhaut, T., Estournel, C., Nguyen, C., & Ulses, C. (2012). Alternatives to the Robert-Asselin filter. *Ocean Modelling*, *41*, 53–66.
- Marsaleix, P., Auclair, F., Estournel, C., Nguyen, C., & Ulses, C. (2011). An accurate implementation of the compressibility terms in the equation of state in a low order pressure gradient scheme for sigma coordinate ocean models. *Ocean Modelling*, *40*, 1–13. <https://doi.org/10.1016/j.ocemod.2011.07.004>
- Marsaleix, P., Auclair, F., Floor, J. W., Herrmann, M. J., Estournel, C., Pairaud, I., & Ulses, C. (2008). Energy conservation issues in sigma-coordinate free-surface ocean models. *Ocean Modelling*, *20*, 61–89. <https://doi.org/10.1016/j.ocemod.2007.07.005>
- Marsaleix, P., Ulses, C., Pairaud, I., Herrmann, M. J., Floor, J. W., Estournel, C., & Auclair, F. (2009). Open boundary conditions for internal gravity wave modelling using polarization relations. *Ocean Modelling*, *29*, 27–42. <https://doi.org/10.1016/j.ocemod.2009.02.010>
- Marshall, J., & Schott, F. (1999). Open-ocean convection: Observations, theory, and models. *Reviews of Geophysics*, *37*(1), 1–64. <https://doi.org/10.1029/98RG02739>
- Martin, A. P., & Pondaven, P. (2006). New primary production and nitrification in the western subtropical North Atlantic: A modeling study. *Global Biogeochemical Cycles*, *20*, GB4014. <https://doi.org/10.1029/2005GB002608>
- Mayot, N., D'Ortenzio, F., Ribera là, M., Lavigne, H., & Claustre, H. (2016). The Mediterranean trophic regimes from ocean color satellites: A reappraisal. *Biogeoscience*, *13*, 1901–1917. <https://doi.org/10.5194/bg-13-1901-2016>
- Mayot, N., D'Ortenzio, F., Taillandier, V., Prieur, L., Pasquero de Fommervault, O., Claustre, H., . . . Conan, P. (2017). Physical and biogeochemical controls of the phytoplankton blooms in North-Western Mediterranean Sea: A multiplatform approach over a complete annual cycle (2012–2013 DEWEX experiment). *Journal of Geophysical Research: Oceans*, <https://doi.org/10.1002/2016JC012052>, in press.
- MEDOC Group. (1970). Observation of formation of deep water in the Mediterranean Sea. *Nature*, *227*(1037), 1040.
- Mignot, A., Claustre, H., Uitz, J., Poteau, A., D'Ortenzio, F., & Xing, X. (2014). Understanding the seasonal dynamics of phytoplankton biomass and the deep chlorophyll maximum in oligotrophic environments: A Bio-Argo float investigation. *Global Biogeochemical Cycles*, *28*, 856–876. <https://doi.org/10.1002/2013GB004781>
- Moutin, T., Raimbault, P., Golterman, H. L., & Coste, B. (1998). The input of nutrients by the Rhône River into the Mediterranean Sea: Recent observations and comparison with earlier data. *Hydrobiologia*, *373*, 237. <https://doi.org/10.1023/A:1017020818701>
- Nittis, K., Lascaratos, A., & Theocharis, A. (2003). Dense water formation in the Aegean Sea: Numerical simulations during the Eastern Mediterranean Transient. *Journal of Geophysical Research*, *108*(C9), 8120. <https://doi.org/10.1029/2002JC001352>
- Ovchinnikov, I. M. (1984). The formation of Intermediate Water in the Mediterranean. *Oceanology*, *24*, 168–173.
- Pasquero de Fommervault, O., D'Ortenzio, F., Mangin, A., Serra, R., Migon, C., Claustre, H., . . . Obolensky, G. (2015b). Seasonal variability of nutrient concentrations in the Mediterranean Sea: Contribution of Bio-Argo floats. *Journal of Geophysical Research: Oceans*, *120*, 8528–8550. <https://doi.org/10.1002/2015JC011103>
- Palevsky, H. I., Quay, P. D., Lockwood, D. E., & Nicholson, D. P. (2016). The annual cycle of gross primary production, net community production, and export efficiency across the North Pacific Ocean. *Global Biogeochemical Cycles*, *30*. <https://doi.org/10.1002/2015GB005318>
- Pasquero de Fommervault, O., Migon, C., D'Ortenzio, F., Ribera d'Alcalà, M., & Coppola, L. (2015a). Temporal variability of nutrient concentrations in the northwestern Mediterranean sea (DYFAMED time-series station). *Deep Sea Research Part I: Oceanographic Research Papers*, *100*, 1–12.
- Pastor, L., Cathalot, C., Deflandre, B., Viollier, E., Soetaert, K., Meysman, F. J. R., . . . Rabouille, C. (2011). Modeling biogeochemical processes in sediments from the Rhone River prodelta area (NW Mediterranean Sea). *Biogeosciences*, *8*, 1351–1366.
- Petrenko, A., Dufau, C., & Estournel, C. (2008). Barotropic eastward currents in the western Gulf of Lion, north-western Mediterranean Sea, during stratified conditions. *Journal of Marine Systems*, *74*, 406–428. <https://doi.org/10.1016/j.jmarsys.2008.03.004>
- Pollak, M. (1951). The sources of deep water of the Eastern Mediterranean Sea. *Journal of Marine Research*, *10*, 128–152.
- Pujo-Pay, M., & Conan, P. (2003). Seasonal variability and export of dissolved organic nitrogen in the northwestern Mediterranean Sea. *Journal of Geophysical Research*, *108*(C6), 3188. <https://doi.org/10.1029/2000JC000368>
- Pujo-Pay, M., Conan, P., Oriol, L., Cornet-Barthaux, V., Falco, C., Ghiglione, J.-F., . . . Prieur, L. (2011). Integrated survey of elemental stoichiometry (C, N, P) from the western to eastern Mediterranean Sea. *Biogeosciences*, *8*(4), 883–899. <https://doi.org/10.5194/bg-8-883-2011>
- Raimbault, P., & Coste, B. (1990). Very high values of nitrate:phosphate ratio (>30) in the subsurface layers of the western Mediterranean Sea. *Rapp. Comm. Int. Mer. Mediterr.*, *32*(1), C-18.
- Raimbault, P., Slawyk, G., Boudjellal, B., Coatanoan, C., Conan, P., Coste, B., . . . Pujo-Pay, M. (1998). Carbon and nitrogen uptake and export in the equatorial Pacific at 150°W: Evidence of an efficient regenerated production cycle. *Journal of Geophysical Research*, *104*(C2), 3341–3356.
- Redfield, A. C., Ketchum, B. H., & Richards, F. A. (1963). *The influence of organisms on the composition of sea-water* (Contrib. 1113, Woods Hole Oceanographic Institution and Contrib. 238). Seattle: Department of Oceanography, University of Washington.
- Ribera d'Alcalà, M., Civitarese, G., Conversano, F., & Lavezza, R. (2003). Nutrient ratios and fluxes hint at overlooked processes in the Mediterranean Sea. *Journal of Geophysical Research*, *108*(C9), 8106. <https://doi.org/10.1029/2002JC001650>
- Ridame, C., & Guieu, C. (2002). Saharan input of phosphate to the oligotrophic water of the open western Mediterranean Sea. *Limnology and Oceanography*, *47*, 856–869. <https://doi.org/10.4319/lo.2002.47.3.0856>
- Santinelli, C., Ibello, V., Lavezza, R., Civitarese, G., & Seritti, A. (2012). New insights into C, N and P stoichiometry in the Mediterranean Sea: The Adriatic Sea case. *Continental Shelf Research*, *44*, 83–93.

- Sempéré, R., Charrière, B., Van Wambeke, F., & Cauwet, G. (2000). Carbon inputs of the Rhône River to the Mediterranean Sea: Biogeochemical Implications. *Global Biogeochemical Cycles*, *14*(2), 669–681.
- Severin, T., Conan, P., Durrieu de Madron, X., Houpert, L., Oliver, M. J., Oriola, L., . . . Pujo-Pay, M. . . (2014). Impact of open-ocean convection on nutrients, phytoplankton biomass and activity. *Deep Sea Research Part I: Oceanographic Research Papers*, *94*, 62–71. <https://doi.org/10.1016/j.dsr.2014.07.015>
- Severin, T., Kessouri, F., Rembauville, M., Sánchez-Pérez, E. D., Oriol, L., Caparros, J., . . . Conan, P. (2017). Open-ocean convection process: A driver of the winter nutrient supply and the spring phytoplankton distribution in the Northwestern Mediterranean Sea. *Journal of Geophysical Research: Oceans*, *122*, 4587–4601. <https://doi.org/10.1002/2016JC012664>
- Soetaert, K., Herman, P. M. J., Middelburg, J. J., Heip, C., Smith, C. L., Tett, P., & Wild-Allen, K. (2001). Numerical modelling of the shelf break ecosystem: Reproducing benthic and pelagic measurements. *Deep Sea Research Part II: Topical Studies in Oceanography*, *48*, 3141–3177.
- Somot, S., Sevault, F., & Déqué, M. (2006). Transient climate change scenario simulation of the Mediterranean Sea for the 21st century using a high-resolution ocean circulation model. *Climate Dynamics*, *27*, 851–879.
- Testor, P. (2013). *DEWEX-MERMEX 2013 LEG1 cruise, RV Le Suroît*. Brest, France: SISMER. <https://doi.org/10.17600/13020010>
- Testor, P., Coppola, L., & Mortier, L. (2013). *MOOSE-GE 2013 cruise, RV Thétyis II*. Brest, France: SISMER. <https://doi.org/10.17600/13450110>
- Ulses, C., Auger, P.-A., Soetaert, K., Marsaleix, P., Diaz, F., Coppola, L., . . . Estournel, C. (2016). Budget of organic carbon in the North-Western Mediterranean Open Sea over the period 2004–2008 using 3-D coupled physical-biogeochemical modeling. *Journal of Geophysical Research: Oceans*, *121*, 7026–7055. <https://doi.org/10.1002/2016JC011818>
- Ulses, C., Estournel, C., Puig, P., Durrieu de Madron, X., & Marsaleix, P. (2008). Dense shelf water cascading in the northwestern Mediterranean during the cold winter 2005: Quantification of the export through the Gulf of Lion and the Catalan margin. *Geophysical Research Letters*, *35*, L07610. <https://doi.org/10.1029/2008GL033257>
- Williams, R. G., & McLaren, A. J. (2000). Estimating the convective supply of nitrate and implied variability in export production over the North Atlantic. *Global Biogeochemical Cycles*, *14*(4), 1299–1313.
- Yilmaz, A., & Tugrul, S. (1998). The effect of cold- and warm-core eddies on the distribution and stoichiometry of dissolved nutrients in the northeastern Mediterranean. *Journal of Marine Systems*, *16*(3–4), 253–268.